The Astrophysical Journal Supplement Series, 182:51–79, 2009 May doi:10.1088/0067-0049/182/1/51

IMPROVED LABORATORY TRANSITION PROBABILITIES FOR Ce II, APPLICATION TO THE CERIUM ABUNDANCES OF THE SUN AND FIVE *r*-PROCESS-RICH, METAL-POOR STARS, AND RARE EARTH LAB DATA SUMMARY

J. E. Lawler[1], C. Sneden[2,3], J. J. Cowan[4], I. I. Ivans[5,6], and E. A. Den Hartog[1]
[1] Department of Physics, University of Wisconsin, Madison, WI 53706, USA; jelawler@wisc.edu, eadenhar@wisc.edu
[2] Department of Astronomy and McDonald Observatory, University of Texas, Austin, TX 78712, USA
[3] INAF, Osservatorio Astronomico di Padova, Vicolo Osservatorio 5, I-35122 Padova, Italy; chris@verdi.as.utexas.edu
[4] Homer L. Dodge Department of Physics and Astronomy, University of Oklahoma, Norman, OK 73019, USA; cowan@nhn.ou.edu
[5] The Observatories of the Carnegie Institution of Washington, 813 Santa Barbara St., Pasadena, CA 91101, USA
[6] Princeton University Observatory, Peyton Hall, Princeton, NJ 08544, USA; iii@ociw.edu
Received 2008 November 20; accepted 2009 March 16; published 2009 April 15

ABSTRACT

Recent radiative lifetime measurements accurate to ±5% using laser-induced fluorescence (LIF) on 43 even-parity and 15 odd-parity levels of Ce II have been combined with new branching fractions measured using a Fourier transform spectrometer (FTS) to determine transition probabilities for 921 lines of Ce II. This improved laboratory data set has been used to determine a new solar photospheric Ce abundance, log $\varepsilon = 1.61 \pm 0.01$ ($\sigma = 0.06$ from 45 lines), a value in excellent agreement with the recommended meteoritic abundance, log $\varepsilon = 1.61 \pm 0.02$. Revised Ce abundances have also been derived for the *r*-process-rich metal-poor giant stars BD+17°3248, CS 22892–052, CS 31082–001, HD 115444, and HD 221170. Between 26 and 40 lines were used for determining the Ce abundance in these five stars, yielding a small statistical uncertainty of ±0.01 dex similar to the solar result. The relative abundances in the metal-poor stars of Ce and Eu, a nearly pure *r*-process element in the Sun, matches *r*-process-only model predictions for solar system material. This consistent match with small scatter over a wide range of stellar metallicities lends support to these predictions of elemental fractions. A companion paper includes an interpretation of these new precision abundance results for Ce as well as new abundance results and interpretation for Pr, Dy, and Tm.

Key words: atomic data – Galaxy: evolution – nuclear reactions, nucleosynthesis, abundances – stars: abundances – stars: individual (BD+17°3248, CS 22892–052, CS 31082–001, HD 115444, HD 221170) – stars: Population II – Sun: abundances

Online-only material: color figure, machine-readable tables

1. INTRODUCTION

The study of elemental abundances in stellar photospheres continues to be a rich area of investigation. Halo stars are among the oldest objects in the Galaxy and these stars provide a "fossil" record of the Galactic chemical evolution. The discovery and detailed study of a class of metal-poor Galactic halo stars with variable *n*(eutron)-capture elemental abundances (e.g., Sneden et al. 1995; Smith et al. 1995; Cowan et al. 1996; Woolf et al. 1995; Sneden et al. 1996; Burris et al. 2000; Hill et al. 2002, Sneden et al. 2003b) is particularly significant.

Rare-Earth (RE) elements are among the most spectroscopically accessible of the *n*-capture elements. The open f-shell of the RE neutral atoms and ions yields many strong lines in the visible and near-IR where spectral line blending is less of a problem than in the UV, and where ground-based observations are possible. Observations with a high signal-to-noise ratio (S/N) and a high spectral resolving power on an increasing number of stars are now available from large ground-based telescopes. The quality of these new astronomical data can be fully exploited only if similar quality basic spectroscopic data, especially data on transition probabilities, are available. The combination of improved astronomical data and improved laboratory data has reduced line-to-line and star-to-star scatter in abundance values for many RE elements.

Cerium is the last of the RE elements in need of additional work and it has the richest line spectra of the RE elements. Experimental work since the mid-1990s has emphasized laser-induced fluorescence (LIF) lifetime measurements (e.g., Langhans et al. 1995; Li et al. 2000; Zhang et al. 2001; Xu et al. 2003; Den Hartog & Lawler 2008). These LIF lifetimes have typically been combined with theoretical branching fractions to determine transition probabilities for individual Ce II lines (e.g., Zhang et al. 2001; Palmeri et al. 2000; Biémont & Quinet 2005).

In spite of the somewhat daunting line density, a large set of Ce II branching fractions measurements based on Fourier transform spectrometer (FTS) data is now complete. The branching fraction measurements are combined with the most recent and extensive LIF radiative lifetimes from Den Hartog & Lawler (2008) to determine transition probabilities for 921 lines of Ce II reported herein.

Although progress has been made in the theoretical determination of atomic transition probabilities, a recent comparison strongly suggests that modern experimental methods yield more reliable atomic transition probabilities (Lawler et al. 2008a). The method used in this study on Ce is to combine radiative lifetimes from time-resolved LIF (TR-LIF) with emission branching fraction measurements from high resolution data recorded using an FTS. This method for measuring transition probabilities is accurate, flexible, and efficient. The systematic determination of experimental transition probabilities by combining radiative lifetimes from TR-LIF with branching fractions from emission data recorded with an FTS has played a central role in providing the basic atomic data needed for RE abundance determinations. This method yields absolute transition probabilities which are accurate to ±5% (∼0.02 dex) for strong lines.

These laboratory data are applied to re-determine the solar abundance of Ce and to refine the Ce abundance in five *r*-process-rich, metal-poor Galactic halo stars. The Appendix to this paper includes a summary to all of our RE lab data in machine-readable (MR) form. This work on Ce II completes a multi-year effort to improve laboratory spectroscopic data for RE ions and to apply these data in abundance studies (Lawler et al. 2008b and references therein).

The emergence of a tightly defined *r*-process-only abundance pattern in many very metal-poor Galactic halo stars, at least for the RE elements, has been an exciting development (e.g., Sneden et al. 2003a; Ivans et al. 2006; Lawler et al. 2006; Den Hartog et al. 2006). As this abundance pattern becomes even more tightly defined, it will: (1) provide a powerful constraint on future modeling of the *r*-process nucleosynthesis, (2) help determine a definitive *r*-process site, and (3) unlock other details of the *r*-process and of the Galactic chemical evolution.

2. CE II BRANCHING FRACTIONS AND ATOMIC TRANSITION PROBABILITIES

As discussed above, radiative lifetimes from Den Hartog & Lawler (2008) provide a foundation for this study of branching fractions and the transition probabilities of Ce II. Branching fraction measurements were attempted on lines from all 74 levels of the lifetime experiment, and were completed for lines from 43 even-parity and 15 odd-parity upper levels. As in earlier work on other RE spectra, we used the 1.0 m FTS at the National Solar Observatory (NSO) on Kitt Peak for Ce II branching fraction measurements. The Kitt Peak FTS has the large etendue of all interferometric spectrometers, a limit of resolution as small as 0.01 cm^{-1}, wavenumber accuracy to 1 part in 10^8, broad spectral coverage from the UV to IR, and the capability of recording a million point spectrum in 10 minutes (Brault 1976). The line density in Ce II is so high that a very high performance FTS is essential. Grating spectrographs are not adequate.

2.1. Energy Levels of Ce II

Figure 1 shows a partial Grotrian diagram constructed from the energy level compilation of Martin et al. (1978) for singly ionized Ce. A total of 288 even-parity and 192 odd-parity levels are included in the compilation. Most of the low-lying ($< 20{,}000$ cm^{-1}) energy levels are known and have assignments. Although Ce II is the most complex of the singly ionized RE spectra, classical analyses of the spectrum have yielded extensive results (e.g., Martin et al. and reference therein). The absence of hyperfine structure (hfs) results in narrow spectral lines and a tolerable amount of line blending for such a rich spectrum.

There are three low odd-parity configurations including the $4f(^2F)5d^2$, $4f(^2F)6s^2$, and $4f(^2F)5d6s$ which contribute over 100 levels below 20,000 cm^{-1} including the ground level. This near degeneracy of the 4f, 5d, and 6s orbitals is typical of REs and it leads to substantial configuration mixing. Of the 118 low-lying odd-parity levels listed in Martin et al. (1978), 74 are assigned to the $4f(^2F)5d^2$ configuration, two are assigned to the $4f(^2F)6s^2$ configuration, and 42 are assigned to the $4f(^2F)5d6s$ configuration. Not all of these 118 levels have term assignments, but a counting of angular momentum projections indicates that very few (perhaps only 2) levels from these three configurations are unobserved. There is a gap of about 5700 cm^{-1} before the $4f^26p$ configuration starts at 25,766 cm^{-1}. The nearly complete knowledge of low odd-parity levels simplifies the branching fraction study, since there is little chance of missing a strong branch to an unobserved lower level. Even-parity upper levels of this study are between 24,000 and 33,000 cm^{-1} and all have short, < 9 ns, radiative lifetimes. Due to the frequency cubed scaling of transition probabilities, there is no real possibility of near-IR branches to higher unobserved levels contributing more than a small fraction of 1% to the total decay of such short lived levels.

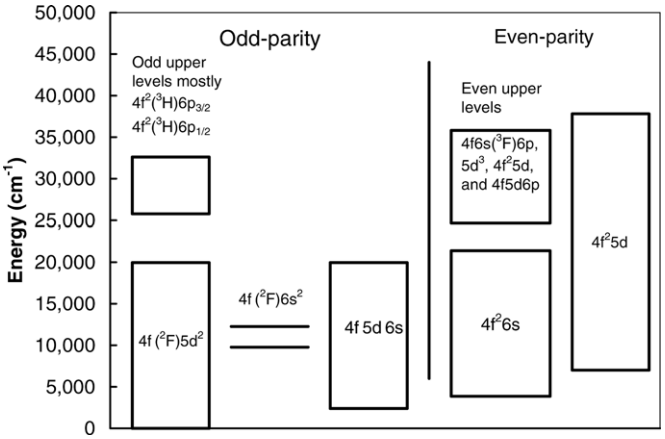

Figure 1. Partial Grotrian diagram for Ce II. Upper and lower levels of both parities included in this study are shown.

Two configurations, the $4f^26s$ and $4f^25d$, contribute low-lying even-parity levels. Although the $4f^26s$ configuration extends from 3800 cm^{-1} to just over 21,000 cm^{-1}, the $4f^25d$ extends up to nearly 40,000 cm^{-1}. There are 99 known even-parity levels below 25,000 cm^{-1}. A counting of angular momentum projections including levels of the $4f^25d$ configuration up to 40,000 cm^{-1} indicates that few (perhaps only 4) levels of the two low even-parity configurations are unobserved. These unobserved even-parity levels are low J levels (3/2 or 1/2) and are likely around 20,000 cm^{-1} or higher. Two of the missing $J = 1/2$ levels were found by Palmeri et al. (2000). This situation is similar to the other parity; there is a nearly complete knowledge of low even-parity levels. Odd-parity upper levels of this study are between 25,000 and 33,000 cm^{-1} and all have short, < 9 ns, radiative lifetimes. Due to the frequency cubed scaling of transition probabilities, there is again no possibility of near-IR branches to higher unobserved levels contributing more than a small fraction of 1% to the total decay of such short lived levels. This nearly complete knowledge, including assignments, of the low-lying ($< 20{,}000$ cm^{-1}) energy levels of both parities in Ce II greatly simplifies the branching fraction analysis.

2.2. Ce II Branching Fraction Analysis and Relative Radiometric Calibration

As in earlier studies our experimental branching fractions are based on a large set of FTS data including: spectra of lamps at high currents to reveal very weak branches to known levels, good IR spectra to reveal weak IR branches to known levels, and low current spectra in which dominant branches are optically thin covering the UV to near-IR. Table 1 is a list of the 14 FTS spectra used in our branching fraction study. All were recorded using the National Solar Observatory 1.0 m FTS on Kitt Peak. Most of these spectra, #1–9, were recorded during a February 2002 observing run using Hollow Cathode Discharge (HCD) lamps. Visible spectra of an Electrodeless Discharge Lamp (EDL), #10–11, have quite good S/N on weaker lines. Lines

Table 1
Fourier Transform Spectra of Ce Lamps used in This Study. All Were Recorded Using the 1.0 m FTS on the McMath Telescope at the National Solar Observatory, Kitt Peak, AZ

Index	Date	Serial Number	Lamp Type[a]	Buffer Gas	Lamp Current (mA)	Wavenumber Range (cm^{-1})	Limit of Resolution (cm^{-1})	Coadds	Beam Splitter	Filter	Detector[b]	Calibration[c]
1	2002 Feb 27	30	Commercial HCD	Ar	27	7929–34998	0.050	50	UV		S. B. Si Diode	Ar I & II WQH Lamp
2	2002 Feb 28	32	Commercial HCD	Ar	27	7929–34998	0.050	50	UV		S. B. Si Diode	Ar I & II WQH Lamp
3	2002 Feb 28	33	Commercial HCD	Ar	27	7929–34998	0.050	112	UV		S. B. Si Diode	Ar I & II WQH Lamp
4	2002 Feb 27	29	Commercial HCD	Ar	27	7929–34998	0.050	8	UV		S. B. Si Diode	Ar I & II WQH Lamp
5	2002 Feb 26	14	Commercial HCD	Ar	22	7929–34998	0.050	10	UV		S. B. Si Diode	Ar I & II WQH Lamp
6	2002 Feb 26	15	Commercial HCD	Ar	17	7929–34998	0.050	10	UV		S. B. Si Diode	Ar I & II WQH Lamp
7	2002 Feb 27	28	Commercial HCD	Ne	27	7929–34998	0.050	9	UV		S. B. Si Diode	WQH Lamp
8	2002 Feb 26	16	Commercial HCD	Ne	25	7929–34998	0.050	10	UV		S. B. Si Diode	WQH Lamp
9	2002 Feb 27	20	Commercial HCD	Ne	20	7929–34998	0.050	20	UV		S. B. Si Diode	WQH Lamp
10	1985 Feb 5	23	EDL CeI_3	Ar	...	7456–28808	0.035	8	UV	GG375	S. B. Si Diode	W Strip Lamp
11	1985 Feb 5	67	EDL CeI_3	Ar	...	7456–28808	0.035	8	UV	GG375	S. B. Si Diode	W Strip Lamp
12	1985 Feb 5	4	EDL CeI_3	Ar	...	3285–15050	0.018	3	UV	RG715	InSb	W Strip Lamp
13	1985 Feb 5	5	EDL CeI_3	Ar	...	3285–15050	0.018	5	UV	RG715	InSb	W Strip Lamp
14	1985 Feb 6	35	EDL CeI_3	Ar	...	3285–15050	0.018	11	UV	RG715	InSb	W Strip Lamp

Notes.
[a] Lamp types include commercially available small sealed hollow cathode discharge (HCD) lamps typically used in atomic absorption spectrophotometers and an electrodeless discharge lamp (EDL) run with isotopically pure ^{140}Ce introduced as an iodide salt.
[b] Detectors types include the super blue (S. B.) Si photodiode and Indium antimonide (InSb) detector for the near infrared.
[c] Relative radiometric calibrations were based on selected sets of Ar I and Ar II lines, on a tungsten–quartz–halogen (WQH) lamp calibrated as a secondary irradiance standard, and on a tungsten (W) Strip Lamp calibrated as a secondary radiance standard.

of Ce II in comparison to lines of Ce I are stronger in spectra #10–11 than in spectra #1–9 and this effect was very valuable in assessing possible blends of Ce II and Ce I lines. Spectra of Ce/Ne HCD lamps were used only to assess and, when necessary, correct for blends between Ce II and Ar lines. Since no Ar II or Ar I lines appeared in the EDL spectra, these could also be used to assess and correct for blends between Ce II and Ar lines. This redundancy is important since many cases of possible blends involving Ce II, Ce I, and Ar lines occur. No significant optical depth effects on Ce II lines appear in any of the spectra, probably due to the rich level structure and large partition function of this ion. Spectra #12–14 yielded measurements on a few near-IR lines, but generally the near IR lines from the short lived levels of this study have negligible branching fractions. All 14 raw spectra are available from the electronic archives of the National Solar Observatory.[7]

The establishment of an accurate relative radiometric calibration or efficiency is critical to a branching fraction experiment. As indicated in Table 1, we made use of both standard lamp calibrations and Ar I and Ar II line calibrations in this Ce II study. Tungsten (W) filament standard lamps are particularly useful near the Si detector cutoff in the 10,000 to 9000 cm^{-1} range where the FTS sensitivity is changing rapidly as a function of wavenumber, and near the dip in sensitivity at 12,500 cm^{-1} from the aluminum coated optics. Tungsten lamps are not bright enough to be useful for FTS calibrations in the UV region, and blue or UV branches typically dominate the decay of levels studied using our lifetime experiment. In general one must be careful when using continuum lamps to calibrate the FTS over wide spectral ranges, because the "ghost" of a continuum is a continuum. The Ar I and Ar II line technique, which is internal to the HCD Ce/Ar lamp spectra, is still our preferred calibration technique. It captures the wavelength-dependent response of detectors, spectrometer optics, lamp windows, and any other components in the light path or any reflections which contribute to the detected signal (such as due to light reflecting off the back of the hollow cathode). This calibration technique is based on a comparison of well-known branching ratios for sets of Ar I and Ar II lines widely separated in wavelength, to the intensities measured for the same lines. Sets of Ar I and Ar II lines have been established for this purpose in the range of 4300–35000 cm^{-1} by Adams & Whaling (1981); Danzmann & Kock (1982); Hashiguchi & Hasikuni (1985), and Whaling et al. (1993). The Ce/Ne spectra from 2002 and the EDL spectra from 1985 could only be calibrated using W standard lamps. The older W lamp is a strip lamp calibrated as a spectral radiance (Watts $(m^2$ sr $nm)^{-1}$) standard, and the newer is a tungsten-quartz-halogen lamp calibrated as a spectral irradiance (Watts $(m^2$ $nm)^{-1}$ at a specified distance) standard. Neither of these W filament lamps is hot or bright enough to yield a reliable UV calibration, but they are useful in the visible and near IR for interpolation and as a redundant calibration.

[7] Available at http://nsokp.nso.edu/.

All possible transition wavenumbers between known energy levels of Ce II satisfying both the parity change and $\Delta J = -1$, 0, or 1 selection rules were computed and used during analysis of FTS data. Energy levels from Martin et al. (1978) were used to determine possible transition wavenumbers. Levels from Martin et al. (1978) are available in electronic form from Martin et al. (2000).[8] Systematic errors from missing branches to known lower levels are negligible in our work, because the level structure of Ce II is so well known and because we were able to make measurements on branching fractions of 0.01 or smaller. All naturally occurring Ce isotopes are even (nuclear spin $I = 0$) isotopes: ^{136}Ce (abundance 0.185%), ^{138}Ce (abundance 0.251%), ^{140}Ce (abundance 88.450%), and ^{142}Ce (abundance 11.114%) (Böhlke et al. 2005). Lines of Ce II are generally quite narrow because they have no hfs and small isotope shifts.

Branching fraction measurements were completed for lines from 43 even-parity and 15 odd-parity upper levels of the 74 levels studied in the lifetime experiment by Den Hartog & Lawler (2008). The levels for which branching fractions could not be completed had a strong branch beyond the UV limit of our spectra, or had a strong branch which was severely blended. Typically an even-parity upper level, depending on its J value, has about 55 possible transitions to known lower levels, and an odd-parity upper level has about 40 possible transitions to known lower levels. More than 30,000 possible spectral line observations were studied during the analysis of 14 different Ce/Ar and Ce/Ne spectra. We set integration limits and occasionally nonzero baselines "interactively" during analysis of the FTS spectra. An occasional nonzero baseline is needed when a weak line is located on a line wing of a much stronger line. Weak red and near-IR lines of Ce II in the EDL spectra also require a nonzero baseline due to some continuum emission from this lamp. The same numerical integration routine was used to determine the un-calibrated intensities of Ce II lines and selected Ar I and Ar II lines used to establish a relative radiometric calibration of the spectra. A simple numerical integration technique was used in this and most of our other RE studies because of weakly resolved or unresolved hyperfine and isotopic structure. More sophisticated profile fitting is used only when the line subcomponent structure is either fully resolved in the FTS data or known from independent measurements.

2.3. Branching Fraction Uncertainties

The procedure for determining branching fraction uncertainties was described in detail by Wickliffe et al. (2000). Branching fractions from a given upper level are defined to sum to unity, thus a dominant line from an upper level has small branching fraction uncertainty almost by definition. Branching fractions for weaker lines near the dominant line(s) tend to have uncertainties limited by their S/N. Systematic uncertainties in the radiometric calibration are typically the dominant source of uncertainty for widely separated lines from a common upper level. We used a formula for estimating this systematic uncertainty that was presented and tested extensively by Wickliffe et al. (2000). The EDL spectra enabled us to include measurements of quite weak branches in the visible and near-IR. Uncertainties on branching fractions of the weak visible and near-IR lines are larger than uncertainties on the dominant branches. In the final analysis, the branching fraction uncertainties are primarily systematic. Redundant measurements with independent radiometric calibrations help in the assessment of systematic uncertainties. Redundant measurements from spectra with different discharge conditions also make it easier to spot blended lines. Typically some fraction of a weak blended feature with a 1% or less branching fraction was included in the branching fraction normalization, but the blended line was omitted from the final table of transition probabilities.

2.4. Ce II Atomic Transition Probabilities

Branching fractions from the FTS spectra were combined with the radiative lifetime measurements (Den Hartog & Lawler 2008) to determine absolute transition probabilities for 921 lines of Ce II in Table 2. Air wavelengths in Table 2 were computed from energy levels (Martin et al. 1978) using the standard index of air (Edlén 1953). Parities are included in Table 2 using "ev" and "od" notation and decimal notation for J values which are compatible with our MR table of transition probabilities.

Transition probabilities for the very weakest lines (branching fractions ~ 0.001 or weaker) which were observed with poor S/N and for weak blended lines (branching fractions $\leqslant 0.01$) are not included in Table 2; however, these lines are included in the branching fraction normalization. The effect of the problem lines becomes apparent if one sums all transition probabilities in Table 2 from a chosen upper level, and compares the sum to the inverse of the upper level lifetime from Den Hartog & Lawler (2008). Typically the sum of the Table 2 transition probabilities is between 90% and 100% of the inverse lifetime. Although there is significant fractional uncertainty in the branching fractions for these problem lines, this does not have much effect on the uncertainty of the stronger lines that were kept in Table 2. Branching fraction uncertainties are combined in quadrature with lifetime uncertainties to determine the transition probability uncertainties in Table 2.

2.5. Comparisons to Other Data Sets

Three large-scale theoretical or semiempirical sets of Ce II transition probabilities are available for comparison to our new experimental results. Figure 2 shows comparisons of our new experimental transition probabilities to theoretical values from Fawcett (1990). A total of 686 lines in common are included in the Fawcett comparisons. Fawcett's results are based on ab initio calculations of Slater parameters which were least-square adjusted to experimental energies. He also included configuration mixing. Figure 3 shows comparisons of our results to theoretical transition probabilities recently downloaded from the DREAM database (Biémont & Quinet 2005).[9] Earlier work by some of the same team members (Palmeri et al. 2000; Zhang et al. 2001) is included in the more extensive online data set. A total of 890 lines in common are included in the Biémont comparisons. The DREAM results may not be purely theoretical due to the use of experimental LIF lifetimes to re-scale theoretical transition probabilities in some cases (e.g., Zhang et al. 2001). Figure 4 shows comparisons of our results to recently downloaded semiempirical results from Kurucz (1998).[10] A total of 529 lines in common are included in the Kurucz comparisons. It is interesting that the comparisons to semiempirical results from Kurucz show the best agreement. It is not possible to draw conclusions about a particular theoretical method because the Kurucz database includes data from a number of sources.

[8] Available at http://physics.nist.gov/PhysRefData/ASD/index.html.

[9] Available at http://w3.umh.ac.be/~astro/dream.shtml.

[10] Available at http://kurucz.harvard.edu/.

Table 2
Atomic Transition Probabilities for Ce II Organized by Increasing Wavelength in Air, λ_{air}

λ_{air} (Å)	E_{upper} (cm^{-1})	Parity	J_{upp}	E_{lower} (cm^{-1})	Parity	J_{low}	A-value (10^6 s^{-1})	log(gf)
3422.705	32802.165	ev	5.5	3593.882	od	4.5	19.4 ± 2.4	−0.39
3426.205	30166.057	ev	3.5	987.611	od	4.5	15.5 ± 1.5	−0.66
3485.053	28685.758	ev	2.5	0.000	od	3.5	24.9 ± 1.5	−0.57
3507.941	29908.904	ev	4.5	1410.304	od	4.5	6.0 ± 1.0	−0.96
3520.520	29807.078	ev	3.5	1410.304	od	4.5	8.3 ± 0.8	−0.91
3530.019	30702.610	ev	4.5	2382.246	od	4.5	8.6 ± 0.9	−0.80
3534.045	32492.038	ev	5.5	4203.934	od	6.5	32.4 ± 2.7	−0.14
3539.079	30829.124	ev	3.5	2581.257	od	4.5	35.7 ± 2.7	−0.27
3552.724	30702.610	ev	4.5	2563.233	od	5.5	9.8 ± 0.9	−0.73
3555.001	30702.610	ev	4.5	2581.257	od	4.5	15.5 ± 1.5	−0.53
3560.802	33531.388	ev	6.5	5455.845	od	7.5	73 ± 4	0.29
3577.456	31738.484	ev	5.5	3793.634	od	6.5	60 ± 4	0.14
3580.565	29794.517	ev	3.5	1873.934	od	3.5	3.3 ± 0.4	−1.30
3604.195	28725.148	ev	4.5	987.611	od	4.5	2.6 ± 0.4	−1.30
3632.092	30166.057	ev	3.5	2641.559	od	3.5	7.1 ± 0.8	−0.95
3646.962	29794.517	ev	3.5	2382.246	od	4.5	15.0 ± 1.3	−0.62
3653.104	30245.878	ev	4.5	2879.695	od	5.5	16.2 ± 1.8	−0.49
3653.664	31155.623	ev	6.5	3793.634	od	6.5	22.8 ± 1.6	−0.20
3654.934	29994.041	ev	2.5	2641.559	od	3.5	12.5 ± 1.4	−0.82
3655.844	29908.904	ev	4.5	2563.233	od	5.5	44.9 ± 2.6	−0.05
3658.256	29908.904	ev	4.5	2581.257	od	4.5	1.95 ± 0.21	−1.41
3659.225	28730.712	ev	3.5	1410.304	od	4.5	13.2 ± 1.0	−0.67
3659.970	28725.148	ev	4.5	1410.304	od	4.5	9.2 ± 1.0	−0.73
3660.638	28297.473	ev	3.5	987.611	od	4.5	19.8 ± 1.4	−0.50
3661.907	30180.096	ev	6.5	2879.695	od	5.5	1.32 ± 0.12	−1.43
3665.488	30637.157	ev	2.5	3363.427	od	2.5	1.10 ± 0.18	−1.88
3666.346	29908.904	ev	4.5	2641.559	od	3.5	0.97 ± 0.11	−1.71
3667.978	30134.910	ev	5.5	2879.695	od	5.5	28.2 ± 1.9	−0.17
3668.724	27249.669	ev	2.5	0.000	od	3.5	4.8 ± 0.4	−1.23
3670.668	30829.124	ev	3.5	3593.882	od	4.5	2.15 ± 0.19	−1.46
3671.938	29807.078	ev	3.5	2581.257	od	4.5	5.5 ± 0.6	−1.05
3672.155	28634.516	ev	5.5	1410.304	od	4.5	3.0 ± 0.5	−1.14
3673.633	29794.517	ev	3.5	2581.257	od	4.5	6.2 ± 0.6	−1.00
3679.156	29807.078	ev	3.5	2634.666	od	2.5	4.24 ± 0.28	−1.16
3680.089	29807.078	ev	3.5	2641.559	od	3.5	6.4 ± 0.5	−0.98
3680.857	29794.517	ev	3.5	2634.666	od	2.5	2.17 ± 0.14	−1.45
3682.083	32802.165	ev	5.5	5651.357	od	5.5	6.2 ± 0.7	−0.82
3685.515	30829.124	ev	3.5	3703.594	od	3.5	1.48 ± 0.17	−1.62
3687.799	30702.610	ev	4.5	3593.882	od	4.5	5.9 ± 0.4	−0.92
3694.908	29438.817	ev	5.5	2382.246	od	4.5	5.0 ± 0.5	−0.91
3702.785	30702.610	ev	4.5	3703.594	od	3.5	4.2 ± 0.4	−1.06
3704.976	32802.165	ev	5.5	5819.113	od	4.5	6.2 ± 0.8	−0.81
3709.287	31155.623	ev	6.5	4203.934	od	6.5	29.4 ± 1.8	−0.07
3709.929	27934.638	ev	4.5	987.611	od	4.5	26.3 ± 1.5	−0.26
3716.366	26900.354	ev	3.5	0.000	od	3.5	31.0 ± 1.9	−0.29
3719.791	29438.817	ev	5.5	2563.233	od	5.5	8.0 ± 0.8	−0.70
3722.100	32372.621	od	4.5	5513.709	ev	5.5	6.0 ± 0.6	−0.90
3722.288	29438.817	ev	5.5	2581.257	od	4.5	5.2 ± 0.3	−0.89
3722.763	29449.778	ev	1.5	2595.644	od	1.5	9.3 ± 0.6	−1.11
3724.629	32492.038	ev	5.5	5651.357	od	5.5	6.2 ± 0.5	−0.81
3725.603	30829.124	ev	3.5	3995.460	od	3.5	1.28 ± 0.15	−1.67
3725.673	32802.165	ev	5.5	5969.007	od	5.5	20.0 ± 2.2	−0.30
3726.456	31738.484	ev	5.5	4910.963	od	5.5	1.75 ± 0.18	−1.36
3726.961	27811.496	ev	3.5	987.611	od	4.5	6.3 ± 0.5	−0.98
3728.018	32492.038	ev	5.5	5675.763	od	4.5	29.0 ± 2.3	−0.14
3728.180	29449.778	ev	1.5	2634.666	od	2.5	12.1 ± 1.1	−0.99
3728.417	32269.252	ev	7.5	5455.845	od	7.5	43.1 ± 2.9	0.16
3728.637	28685.758	ev	2.5	1873.934	od	3.5	3.05 ± 0.28	−1.42
3729.916	30166.057	ev	3.5	3363.427	od	2.5	3.1 ± 0.3	−1.29
3732.462	29166.597	ev	4.5	2382.246	od	4.5	2.43 ± 0.21	−1.29
3736.434	32372.621	od	4.5	5616.739	ev	4.5	2.13 ± 0.24	−1.35
3744.010	30065.164	ev	3.5	3363.427	od	2.5	1.75 ± 0.17	−1.53
3746.256	29281.374	ev	2.5	2595.644	od	1.5	2.19 ± 0.17	−1.56
3748.055	32492.038	ev	5.5	5819.113	od	4.5	17.8 ± 1.1	−0.35
3750.998	30245.878	ev	4.5	3593.882	od	4.5	6.5 ± 0.5	−0.86
3751.742	29281.374	ev	2.5	2634.666	od	2.5	2.19 ± 0.16	−1.56

Table 2
(Continued)

λ_{air} (Å)	E_{upper} (cm^{-1})	Parity	J_{upp}	E_{lower} (cm^{-1})	Parity	J_{low}	A-value (10^6 s^{-1})	log(gf)
3752.448	30637.157	ev	2.5	3995.460	od	3.5	3.5 ± 0.3	−1.35
3755.789	33531.388	ev	6.5	6913.392	od	6.5	3.3 ± 0.5	−1.01
3757.855	29166.597	ev	4.5	2563.233	od	5.5	6.8 ± 0.8	−0.84
3760.403	29166.597	ev	4.5	2581.257	od	4.5	1.39 ± 0.13	−1.53
3763.604	30829.124	ev	3.5	4266.397	od	3.5	6.9 ± 0.5	−0.93
3764.115	29438.817	ev	5.5	2879.695	od	5.5	21.4 ± 1.3	−0.26
3766.503	30245.878	ev	4.5	3703.594	od	3.5	5.5 ± 0.4	−0.94
3766.681	30134.910	ev	5.5	3593.882	od	4.5	1.66 ± 0.17	−1.37
3769.052	27934.638	ev	4.5	1410.304	od	4.5	1.51 ± 0.14	−1.49
3771.600	30829.124	ev	3.5	4322.708	od	2.5	16.7 ± 1.0	−0.55
3776.606	30065.164	ev	3.5	3593.882	od	4.5	10.0 ± 0.7	−0.77
3777.662	28337.814	ev	2.5	1873.934	od	3.5	5.8 ± 0.6	−1.13
3781.616	30702.610	ev	4.5	4266.397	od	3.5	25.6 ± 1.4	−0.26
3786.632	27811.496	ev	3.5	1410.304	od	4.5	25.1 ± 1.3	−0.36
3787.903	27379.949	ev	5.5	987.611	od	4.5	4.03 ± 0.28	−0.98
3788.746	30180.096	ev	6.5	3793.634	od	6.5	16.5 ± 1.1	−0.30
3791.002	30637.157	ev	2.5	4266.397	od	3.5	1.48 ± 0.15	−1.72
3791.219	30829.124	ev	3.5	4459.872	od	3.5	1.43 ± 0.15	−1.61
3792.324	30065.164	ev	3.5	3703.594	od	3.5	18.1 ± 1.2	−0.51
3794.210	28730.712	ev	3.5	2382.246	od	4.5	1.48 ± 0.12	−1.59
3795.011	28725.148	ev	4.5	2382.246	od	4.5	5.9 ± 0.4	−0.89
3795.246	30134.910	ev	5.5	3793.634	od	6.5	6.7 ± 0.5	−0.76
3799.032	29908.904	ev	4.5	3593.882	od	4.5	2.51 ± 0.16	−1.26
3800.322	30829.124	ev	3.5	4523.033	od	4.5	8.2 ± 0.6	−0.85
3801.526	33531.388	ev	6.5	7233.627	od	5.5	139 ± 7	0.63
3803.096	29166.597	ev	4.5	2879.695	od	5.5	24.9 ± 1.7	−0.27
3808.113	28634.516	ev	5.5	2382.246	od	4.5	27.7 ± 1.6	−0.14
3808.382	30245.878	ev	4.5	3995.460	od	3.5	1.33 ± 0.12	−1.54
3809.218	31155.623	ev	6.5	4910.963	od	5.5	20.3 ± 1.3	−0.21
3809.497	30702.610	ev	4.5	4459.872	od	3.5	4.6 ± 0.6	−1.00
3814.938	29908.904	ev	4.5	3703.594	od	3.5	2.15 ± 0.16	−1.33
3815.793	27187.047	ev	3.5	987.611	od	4.5	15.1 ± 1.1	−0.58
3818.688	30702.610	ev	4.5	4523.033	od	4.5	4.19 ± 0.30	−1.04
3819.022	30637.157	ev	2.5	4459.872	od	3.5	27.2 ± 2.6	−0.45
3819.998	30166.057	ev	3.5	3995.460	od	3.5	2.08 ± 0.17	−1.44
3821.266	28725.148	ev	4.5	2563.233	od	5.5	7.6 ± 0.4	−0.78
3823.900	28725.148	ev	4.5	2581.257	od	4.5	15.1 ± 1.1	−0.48
3826.534	30637.157	ev	2.5	4511.257	od	2.5	2.7 ± 0.5	−1.44
3829.820	29807.078	ev	3.5	3703.594	od	3.5	1.73 ± 0.21	−1.52
3830.023	32492.038	ev	5.5	6389.942	od	4.5	8.3 ± 0.5	−0.66
3830.911	28730.712	ev	3.5	2634.666	od	2.5	9.3 ± 0.6	−0.79
3831.542	30829.124	ev	3.5	4737.373	od	2.5	6.0 ± 1.0	−0.98
3831.663	29794.517	ev	3.5	3703.594	od	3.5	4.1 ± 0.4	−1.15
3831.782	28685.758	ev	2.5	2595.644	od	1.5	4.7 ± 0.4	−1.21
3832.221	31738.484	ev	5.5	5651.357	od	5.5	8.1 ± 0.7	−0.67
3832.335	29449.778	ev	1.5	3363.427	od	2.5	3.88 ± 0.27	−1.47
3832.741	28725.148	ev	4.5	2641.559	od	3.5	3.9 ± 0.4	−1.07
3834.550	28634.516	ev	5.5	2563.233	od	5.5	12.4 ± 0.8	−0.49
3834.782	30065.164	ev	3.5	3995.460	od	3.5	7.9 ± 0.5	−0.86
3836.107	27934.638	ev	4.5	1873.934	od	3.5	8.5 ± 0.5	−0.73
3837.203	28634.516	ev	5.5	2581.257	od	4.5	3.70 ± 0.28	−1.01
3837.522	28685.758	ev	2.5	2634.666	od	2.5	1.30 ± 0.10	−1.76
3838.538	28685.758	ev	2.5	2641.559	od	3.5	55.0 ± 3.0	−0.14
3843.767	33531.388	ev	6.5	7522.622	od	5.5	14.0 ± 1.3	−0.36
3845.273	29994.041	ev	2.5	3995.460	od	3.5	4.2 ± 0.5	−1.25
3848.100	30245.878	ev	4.5	4266.397	od	3.5	13.1 ± 0.9	−0.54
3848.592	30180.096	ev	6.5	4203.934	od	6.5	27.4 ± 1.6	−0.07
3849.558	27379.949	ev	5.5	1410.304	od	4.5	3.7 ± 0.3	−1.01
3852.099	28334.756	ev	4.5	2382.246	od	4.5	3.7 ± 0.3	−1.08
3853.156	25945.396	ev	3.5	0.000	od	3.5	17.5 ± 1.0	−0.51
3854.185	27812.398	ev	2.5	1873.934	od	3.5	43.1 ± 2.3	−0.24
3854.319	27811.496	ev	3.5	1873.934	od	3.5	39.7 ± 2.1	−0.15
3855.298	30134.910	ev	5.5	4203.934	od	6.5	19.5 ± 1.2	−0.28
3857.025	31738.484	ev	5.5	5819.113	od	4.5	21.0 ± 1.9	−0.25
3857.237	29281.374	ev	2.5	3363.427	od	2.5	13.0 ± 0.9	−0.76
3857.641	28297.473	ev	3.5	2382.246	od	4.5	13.0 ± 0.8	−0.63

Table 2
(Continued)

λ_{air} (Å)	E_{upper} (cm^{-1})	Parity	J_{upp}	E_{lower} (cm^{-1})	Parity	J_{low}	A-value (10^6 s^{-1})	log(gf)
3868.133	29438.817	ev	5.5	3593.882	od	4.5	5.7 ± 0.3	−0.81
3870.867	31340.393	od	6.5	5513.709	ev	5.5	5.2 ± 0.4	−0.79
3872.131	30829.124	ev	3.5	5010.870	od	2.5	2.70 ± 0.19	−1.31
3873.126	29807.078	ev	3.5	3995.460	od	3.5	1.55 ± 0.11	−1.55
3875.012	29794.517	ev	3.5	3995.460	od	3.5	8.0 ± 0.7	−0.84
3875.056	30065.164	ev	3.5	4266.397	od	3.5	10.2 ± 0.7	−0.74
3875.995	30637.157	ev	2.5	4844.644	od	1.5	2.24 ± 0.18	−1.52
3876.126	30702.610	ev	4.5	4910.963	od	5.5	11.7 ± 0.8	−0.58
3878.367	27187.047	ev	3.5	1410.304	od	4.5	24.9 ± 1.5	−0.35
3879.460	31738.484	ev	5.5	5969.007	od	5.5	0.60 ± 0.08	−1.79
3881.668	28634.516	ev	5.5	2879.695	od	5.5	6.7 ± 0.5	−0.74
3881.867	28334.756	ev	4.5	2581.257	od	4.5	7.1 ± 1.4	−0.79
3882.445	28345.313	ev	0.5	2595.644	od	1.5	144 ± 7	−0.19
3883.437	32802.165	ev	5.5	7059.072	od	4.5	2.08 ± 0.23	−1.25
3883.533	30065.164	ev	3.5	4322.708	od	2.5	4.7 ± 0.4	−1.07
3883.576	28337.814	ev	2.5	2595.644	od	1.5	6.7 ± 0.5	−1.04
3885.769	29994.041	ev	2.5	4266.397	od	3.5	3.37 ± 0.25	−1.34
3886.493	30245.878	ev	4.5	4523.033	od	4.5	4.0 ± 0.4	−1.05
3888.387	30829.124	ev	3.5	5118.806	od	2.5	8.6 ± 0.6	−0.80
3889.297	29449.778	ev	1.5	3745.475	od	1.5	7.6 ± 0.6	−1.16
3889.472	28337.814	ev	2.5	2634.666	od	2.5	3.7 ± 0.4	−1.29
3889.982	31155.623	ev	6.5	5455.845	od	7.5	41.9 ± 2.3	0.12
3890.515	28337.814	ev	2.5	2641.559	od	3.5	3.01 ± 0.30	−1.39
3890.744	27835.233	ev	1.5	2140.492	od	0.5	18.4 ± 1.3	−0.78
3890.978	28334.756	ev	4.5	2641.559	od	3.5	7.3 ± 0.5	−0.78
3894.292	29994.041	ev	2.5	4322.708	od	2.5	3.63 ± 0.21	−1.31
3896.633	28297.473	ev	3.5	2641.559	od	3.5	1.41 ± 0.10	−1.59
3896.802	30166.057	ev	3.5	4511.257	od	2.5	29.5 ± 1.6	−0.27
3898.263	29438.817	ev	5.5	3793.634	od	6.5	16.7 ± 1.0	−0.34
3898.670	29908.904	ev	4.5	4266.397	od	3.5	1.28 ± 0.08	−1.53
3903.333	30134.910	ev	5.5	4523.033	od	4.5	6.7 ± 0.4	−0.73
3904.337	30065.164	ev	3.5	4459.872	od	3.5	14.7 ± 1.1	−0.57
3907.434	29750.547	od	5.5	4165.550	ev	4.5	6.5 ± 0.4	−0.75
3908.404	32492.038	ev	5.5	6913.392	od	6.5	42.4 ± 2.5	0.07
3908.536	29281.374	ev	2.5	3703.594	od	3.5	23.9 ± 1.3	−0.48
3909.310	29166.597	ev	4.5	3593.882	od	4.5	10.0 ± 0.6	−0.64
3909.747	29735.413	od	4.5	4165.550	ev	4.5	4.78 ± 0.29	−0.96
3912.188	30065.164	ev	3.5	4511.257	od	2.5	15.1 ± 0.9	−0.56
3912.420	27934.638	ev	4.5	2382.246	od	4.5	24.7 ± 1.3	−0.25
3913.992	30065.164	ev	3.5	4523.033	od	4.5	6.6 ± 0.4	−0.92
3914.947	29281.374	ev	2.5	3745.475	od	1.5	5.1 ± 0.3	−1.16
3916.140	29794.517	ev	3.5	4266.397	od	3.5	11.9 ± 0.7	−0.66
3917.639	30637.157	ev	2.5	5118.806	od	2.5	19.9 ± 1.3	−0.56
3919.803	31155.623	ev	6.5	5651.357	od	5.5	22.4 ± 1.5	−0.14
3921.989	26900.354	ev	3.5	1410.304	od	4.5	0.21 ± 0.04	−2.42
3922.863	29807.078	ev	3.5	4322.708	od	2.5	5.7 ± 0.6	−0.98
3923.107	29994.041	ev	2.5	4511.257	od	2.5	44.2 ± 2.5	−0.21
3927.380	28334.756	ev	4.5	2879.695	od	5.5	3.4 ± 0.3	−1.11
3928.310	29908.904	ev	4.5	4459.872	od	3.5	5.9 ± 0.4	−0.86
3930.792	32492.038	ev	5.5	7059.072	od	4.5	9.7 ± 0.7	−0.57
3931.083	26841.384	ev	4.5	1410.304	od	4.5	14.6 ± 0.9	−0.47
3931.366	27811.496	ev	3.5	2382.246	od	4.5	15.4 ± 0.9	−0.54
3937.180	30829.124	ev	3.5	5437.422	od	3.5	0.80 ± 0.08	−1.83
3939.657	27249.669	ev	2.5	1873.934	od	3.5	2.34 ± 0.15	−1.49
3940.330	27934.638	ev	4.5	2563.233	od	5.5	23.3 ± 1.2	−0.27
3940.970	28730.712	ev	3.5	3363.427	od	2.5	14.6 ± 0.9	−0.57
3942.151	25359.686	ev	2.5	0.000	od	3.5	43.1 ± 2.4	−0.22
3942.745	32269.252	ev	7.5	6913.392	od	6.5	132 ± 7	0.69
3943.131	27934.638	ev	4.5	2581.257	od	4.5	7.3 ± 0.4	−0.77
3943.884	31738.484	ev	5.5	6389.942	od	4.5	55 ± 3	0.19
3944.092	29807.078	ev	3.5	4459.872	od	3.5	4.8 ± 0.3	−1.05
3946.047	29794.517	ev	3.5	4459.872	od	3.5	0.39 ± 0.04	−2.14
3947.115	30065.164	ev	3.5	4737.373	od	2.5	1.00 ± 0.10	−1.73
3947.966	28685.758	ev	2.5	3363.427	od	2.5	12.9 ± 0.8	−0.74
3949.404	27187.047	ev	3.5	1873.934	od	3.5	5.0 ± 0.3	−1.03
3952.104	29807.078	ev	3.5	4511.257	od	2.5	5.7 ± 0.5	−0.97

Table 2
(Continued)

λ_{air} (Å)	E_{upper} (cm^{-1})	Parity	J_{upp}	E_{lower} (cm^{-1})	Parity	J_{low}	A-value (10^6 s^{-1})	log(gf)
3952.532	27934.638	ev	4.5	2641.559	od	3.5	33.5 ± 1.7	−0.11
3953.652	29281.374	ev	2.5	3995.460	od	3.5	16.4 ± 0.9	−0.64
3953.944	29807.078	ev	3.5	4523.033	od	4.5	5.3 ± 0.4	−1.00
3955.910	29794.517	ev	3.5	4523.033	od	4.5	8.7 ± 0.8	−0.79
3956.278	30180.096	ev	6.5	4910.963	od	5.5	39.8 ± 2.1	0.12
3956.896	30702.610	ev	4.5	5437.422	od	3.5	10.4 ± 0.6	−0.61
3957.957	32492.038	ev	5.5	7233.627	od	5.5	10.3 ± 1.2	−0.54
3959.607	29449.778	ev	1.5	4201.893	od	1.5	16.6 ± 1.4	−0.81
3960.909	27835.233	ev	1.5	2595.644	od	1.5	45.9 ± 2.4	−0.36
3961.648	29438.817	ev	5.5	4203.934	od	6.5	1.45 ± 0.14	−1.39
3963.365	30134.910	ev	5.5	4910.963	od	5.5	2.86 ± 0.23	−1.09
3964.496	27812.398	ev	2.5	2595.644	od	1.5	15.7 ± 0.9	−0.65
3967.042	27835.233	ev	1.5	2634.666	od	2.5	47.4 ± 2.4	−0.35
3967.173	30637.157	ev	2.5	5437.422	od	3.5	18.5 ± 1.2	−0.58
3967.431	32492.038	ev	5.5	7293.938	od	6.5	0.85 ± 0.08	−1.62
3969.240	31155.623	ev	6.5	5969.007	od	5.5	2.2 ± 0.3	−1.14
3970.640	27812.398	ev	2.5	2634.666	od	2.5	7.5 ± 0.5	−0.97
3970.783	27811.496	ev	3.5	2634.666	od	2.5	0.61 ± 0.04	−1.94
3971.681	29166.597	ev	4.5	3995.460	od	3.5	16.4 ± 0.9	−0.41
3971.870	27811.496	ev	3.5	2641.559	od	3.5	4.3 ± 0.4	−1.09
3974.199	30166.057	ev	3.5	5010.870	od	2.5	3.6 ± 0.3	−1.16
3974.488	30829.124	ev	3.5	5675.763	od	4.5	1.07 ± 0.11	−1.69
3978.646	29449.778	ev	1.5	4322.708	od	2.5	60 ± 3	−0.24
3980.890	30829.124	ev	3.5	5716.216	od	3.5	32.2 ± 2.1	−0.21
3982.901	31738.484	ev	5.5	6638.258	od	4.5	18.1 ± 2.5	−0.29
3983.288	29263.338	od	5.5	4165.550	ev	4.5	8.9 ± 0.6	−0.59
3984.671	32802.165	ev	5.5	7713.089	od	4.5	34.7 ± 2.8	0.00
3990.100	27934.638	ev	4.5	2879.695	od	5.5	4.86 ± 0.27	−0.94
3990.688	30702.610	ev	4.5	5651.357	od	5.5	4.2 ± 0.4	−0.99
3991.325	30166.057	ev	3.5	5118.806	od	2.5	2.30 ± 0.13	−1.36
3992.380	28634.516	ev	5.5	3593.882	od	4.5	20.8 ± 1.1	−0.22
3993.819	32372.621	od	4.5	7341.007	ev	5.5	81 ± 4	0.29
3994.580	30702.610	ev	4.5	5675.763	od	4.5	3.40 ± 0.20	−1.09
3994.648	26900.354	ev	3.5	1873.934	od	3.5	0.49 ± 0.06	−2.02
3995.425	28725.148	ev	4.5	3703.594	od	3.5	0.97 ± 0.07	−1.63
3996.475	29281.374	ev	2.5	4266.397	od	3.5	4.5 ± 0.3	−1.19
3997.269	30829.124	ev	3.5	5819.113	od	4.5	1.18 ± 0.10	−1.64
3999.237	27379.949	ev	5.5	2382.246	od	4.5	39.6 ± 2.0	0.06
4001.047	30702.610	ev	4.5	5716.216	od	3.5	7.6 ± 0.6	−0.74
4001.563	29994.041	ev	2.5	5010.870	od	2.5	17.9 ± 1.4	−0.59
4001.724	28685.758	ev	2.5	3703.594	od	3.5	10.3 ± 0.7	−0.83
4002.822	32269.252	ev	7.5	7293.938	od	6.5	11.4 ± 0.8	−0.36
4002.971	28337.814	ev	2.5	3363.427	od	2.5	5.7 ± 0.5	−1.09
4003.767	32492.038	ev	5.5	7522.622	od	5.5	68 ± 4	0.29
4004.083	26841.384	ev	4.5	1873.934	od	3.5	0.63 ± 0.08	−1.82
4005.492	29281.374	ev	2.5	4322.708	od	2.5	0.43 ± 0.05	−2.20
4005.633	25945.396	ev	3.5	987.611	od	4.5	9.8 ± 0.6	−0.73
4008.444	28685.758	ev	2.5	3745.475	od	1.5	1.70 ± 0.14	−1.61
4011.556	30637.157	ev	2.5	5716.216	od	3.5	6.1 ± 0.7	−1.05
4012.386	29438.817	ev	5.5	4523.033	od	4.5	67 ± 3	0.29
4014.897	29166.597	ev	4.5	4266.397	od	3.5	25.9 ± 1.4	−0.20
4017.135	30829.124	ev	3.5	5942.798	od	3.5	1.54 ± 0.14	−1.53
4017.592	30702.610	ev	4.5	5819.113	od	4.5	4.12 ± 0.24	−1.00
4024.485	28634.516	ev	5.5	3793.634	od	6.5	18.6 ± 1.0	−0.27
4025.139	28345.313	ev	0.5	3508.470	od	0.5	34.5 ± 2.0	−0.78
4027.044	31738.484	ev	5.5	6913.392	od	6.5	2.43 ± 0.23	−1.15
4027.627	29281.374	ev	2.5	4459.872	od	3.5	4.6 ± 0.6	−1.17
4028.404	27379.949	ev	5.5	2563.233	od	5.5	18.5 ± 1.0	−0.27
4031.332	27379.949	ev	5.5	2581.257	od	4.5	19.7 ± 1.1	−0.24
4033.779	29794.517	ev	3.5	5010.870	od	2.5	1.34 ± 0.09	−1.58
4035.982	29281.374	ev	2.5	4511.257	od	2.5	0.47 ± 0.06	−2.17
4037.662	30702.610	ev	4.5	5942.798	od	3.5	14.3 ± 1.0	−0.46
4040.753	28334.756	ev	4.5	3593.882	od	4.5	66 ± 3	0.21
4041.269	30702.610	ev	4.5	5964.896	od	3.5	6.8 ± 0.5	−0.78
4042.581	28725.148	ev	4.5	3995.460	od	3.5	41.1 ± 2.1	0.00
4045.318	30637.157	ev	2.5	5924.204	od	1.5	7.6 ± 0.5	−0.95

Table 2
(Continued)

λ_{air} (Å)	E_{upper} (cm^{-1})	Parity	J_{upp}	E_{lower} (cm^{-1})	Parity	J_{low}	A-value (10^6 s^{-1})	log(gf)
4045.408	29449.778	ev	1.5	4737.373	od	2.5	1.73 ± 0.15	−1.77
4046.338	29166.597	ev	4.5	4459.872	od	3.5	28.5 ± 1.6	−0.16
4046.851	28297.473	ev	3.5	3593.882	od	4.5	0.67 ± 0.08	−1.88
4048.364	30637.157	ev	2.5	5942.798	od	3.5	3.03 ± 0.23	−1.35
4049.362	29807.078	ev	3.5	5118.806	od	2.5	2.5 ± 0.3	−1.31
4051.424	29794.517	ev	3.5	5118.806	od	2.5	9.5 ± 0.8	−0.73
4051.990	30637.157	ev	2.5	5964.896	od	3.5	11.9 ± 1.1	−0.76
4053.503	24663.053	ev	4.5	0.000	od	3.5	10.0 ± 0.5	−0.61
4058.248	28337.814	ev	2.5	3703.594	od	3.5	4.86 ± 0.30	−1.14
4058.751	28334.756	ev	4.5	3703.594	od	3.5	2.29 ± 0.22	−1.25
4061.416	27249.669	ev	2.5	2634.666	od	2.5	1.43 ± 0.23	−1.67
4062.937	27187.047	ev	3.5	2581.257	od	4.5	8.4 ± 0.5	−0.78
4063.045	29449.778	ev	1.5	4844.644	od	1.5	1.89 ± 0.21	−1.73
4063.920	28345.313	ev	0.5	3745.475	od	1.5	16.8 ± 1.0	−1.08
4064.798	30245.878	ev	4.5	5651.357	od	5.5	0.58 ± 0.04	−1.84
4064.904	28297.473	ev	3.5	3703.594	od	3.5	3.23 ± 0.21	−1.19
4068.836	30245.878	ev	4.5	5675.763	od	4.5	27.3 ± 1.5	−0.17
4071.072	29994.041	ev	2.5	5437.422	od	3.5	6.6 ± 0.7	−1.00
4071.775	27187.047	ev	3.5	2634.666	od	2.5	31.5 ± 1.6	−0.20
4072.918	27187.047	ev	3.5	2641.559	od	3.5	11.5 ± 0.6	−0.64
4073.474	28396.150	od	2.5	3854.012	ev	3.5	109 ± 6	0.21
4074.644	25945.396	ev	3.5	1410.304	od	4.5	1.00 ± 0.09	−1.70
4075.546	30245.878	ev	4.5	5716.216	od	3.5	1.80 ± 0.20	−1.35
4075.700	30180.096	ev	6.5	5651.357	od	5.5	48.7 ± 2.5	0.23
4075.847	29438.817	ev	5.5	4910.963	od	5.5	48.6 ± 2.6	0.16
4079.672	31738.484	ev	5.5	7233.627	od	5.5	13.2 ± 1.1	−0.40
4080.438	27379.949	ev	5.5	2879.695	od	5.5	6.7 ± 0.4	−0.70
4082.098	30166.057	ev	3.5	5675.763	od	4.5	1.04 ± 0.11	−1.68
4083.222	30134.910	ev	5.5	5651.357	od	5.5	62 ± 3	0.27
4085.236	29908.904	ev	4.5	5437.422	od	3.5	28.1 ± 1.8	−0.15
4086.433	28730.712	ev	3.5	4266.397	od	3.5	5.3 ± 0.6	−0.97
4087.362	28725.148	ev	4.5	4266.397	od	3.5	7.5 ± 0.4	−0.73
4088.852	30166.057	ev	3.5	5716.216	od	3.5	17.5 ± 1.1	−0.46
4088.997	27812.398	ev	2.5	3363.427	od	2.5	4.62 ± 0.27	−1.16
4089.148	27811.496	ev	3.5	3363.427	od	2.5	1.38 ± 0.11	−1.56
4089.738	31738.484	ev	5.5	7293.938	od	6.5	6.1 ± 0.6	−0.74
4091.046	29281.374	ev	2.5	4844.644	od	1.5	2.70 ± 0.23	−1.39
4092.075	28634.516	ev	5.5	4203.934	od	6.5	2.17 ± 0.25	−1.18
4092.715	30245.878	ev	4.5	5819.113	od	4.5	6.3 ± 0.4	−0.80
4093.956	28685.758	ev	2.5	4266.397	od	3.5	11.7 ± 0.8	−0.75
4098.985	30065.164	ev	3.5	5675.763	od	4.5	9.0 ± 0.7	−0.74
4101.769	31340.393	od	6.5	6967.547	ev	6.5	31.4 ± 1.7	0.05
4106.133	30166.057	ev	3.5	5819.113	od	4.5	6.6 ± 0.4	−0.87
4106.907	28337.814	ev	2.5	3995.460	od	3.5	5.3 ± 0.3	−1.10
4107.177	27934.638	ev	4.5	3593.882	od	4.5	0.35 ± 0.06	−2.05
4107.423	28334.756	ev	4.5	3995.460	od	3.5	28.9 ± 1.5	−0.14
4108.828	29449.778	ev	1.5	5118.806	od	2.5	0.40 ± 0.06	−2.39
4109.539	27835.233	ev	1.5	3508.470	od	0.5	5.1 ± 0.4	−1.28
4110.835	26900.354	ev	3.5	2581.257	od	4.5	4.07 ± 0.28	−1.08
4111.393	30134.910	ev	5.5	5819.113	od	4.5	14.6 ± 1.0	−0.35
4111.922	30702.610	ev	4.5	6389.942	od	4.5	4.35 ± 0.27	−0.96
4113.544	30245.878	ev	4.5	5942.798	od	3.5	1.91 ± 0.20	−1.32
4113.725	28297.473	ev	3.5	3995.460	od	3.5	7.1 ± 0.5	−0.84
4117.288	30245.878	ev	4.5	5964.896	od	3.5	13.9 ± 1.0	−0.45
4117.768	26841.384	ev	4.5	2563.233	od	5.5	0.23 ± 0.04	−2.23
4117.823	29994.041	ev	2.5	5716.216	od	3.5	3.4 ± 0.4	−1.28
4117.985	30245.878	ev	4.5	5969.007	od	5.5	4.3 ± 0.4	−0.96
4118.143	29892.677	od	3.5	5616.739	ev	4.5	66 ± 4	0.13
4119.008	28730.712	ev	3.5	4459.872	od	3.5	14.7 ± 0.8	−0.53
4119.883	26900.354	ev	3.5	2634.666	od	2.5	18.7 ± 1.2	−0.42
4119.953	28725.148	ev	4.5	4459.872	od	3.5	2.30 ± 0.19	−1.23
4120.827	26841.384	ev	4.5	2581.257	od	4.5	16.6 ± 0.9	−0.37
4121.266	29908.904	ev	4.5	5651.357	od	5.5	0.39 ± 0.04	−2.00
4121.591	29166.597	ev	4.5	4910.963	od	5.5	3.08 ± 0.20	−1.11
4123.220	30065.164	ev	3.5	5819.113	od	4.5	15.8 ± 1.3	−0.49
4123.869	31155.623	ev	6.5	6913.392	od	6.5	68 ± 4	0.39
4124.787	29750.547	od	5.5	5513.709	ev	5.5	25.7 ± 1.4	−0.10

Table 2
(Continued)

λ_{air} (Å)	E_{upper} (cm^{-1})	Parity	J_{upp}	E_{lower} (cm^{-1})	Parity	J_{low}	A-value (10^6 s^{-1})	log(gf)
4125.416	29908.904	ev	4.5	5675.763	od	4.5	1.20 ± 0.11	−1.51
4125.773	27934.638	ev	4.5	3703.594	od	3.5	2.67 ± 0.18	−1.17
4126.652	28685.758	ev	2.5	4459.872	od	3.5	7.4 ± 0.6	−0.95
4127.099	30166.057	ev	3.5	5942.798	od	3.5	3.55 ± 0.29	−1.14
4127.364	29735.413	od	4.5	5513.709	ev	5.5	79 ± 4	0.31
4127.748	28730.712	ev	3.5	4511.257	od	2.5	22.4 ± 1.2	−0.34
4128.061	27811.496	ev	3.5	3593.882	od	4.5	11.8 ± 1.1	−0.62
4128.360	31738.484	ev	5.5	7522.622	od	5.5	16.9 ± 1.7	−0.28
4129.174	30180.096	ev	6.5	5969.007	od	5.5	4.6 ± 0.4	−0.78
4130.705	28725.148	ev	4.5	4523.033	od	4.5	24.9 ± 1.3	−0.20
4132.315	29908.904	ev	4.5	5716.216	od	3.5	8.1 ± 0.7	−0.68
4132.626	30829.124	ev	3.5	6638.258	od	4.5	8.9 ± 1.0	−0.74
4135.424	28685.758	ev	2.5	4511.257	od	2.5	21.2 ± 1.4	−0.49
4136.750	29449.778	ev	1.5	5283.029	od	0.5	5.4 ± 0.5	−1.25
4136.895	30134.910	ev	5.5	5969.007	od	5.5	5.9 ± 0.4	−0.74
4137.466	29281.374	ev	2.5	5118.806	od	2.5	21.1 ± 1.3	−0.49
4137.645	28327.071	od	5.5	4165.550	ev	4.5	82 ± 4	0.40
4140.747	28345.313	ev	0.5	4201.893	od	1.5	12.5 ± 0.7	−1.19
4142.034	28337.814	ev	2.5	4201.893	od	1.5	1.82 ± 0.17	−1.55
4142.397	29750.547	od	5.5	5616.739	ev	4.5	54.3 ± 2.8	0.22
4142.825	29807.078	ev	3.5	5675.763	od	4.5	15.6 ± 0.9	−0.49
4144.362	30065.164	ev	3.5	5942.798	od	3.5	3.40 ± 0.23	−1.15
4144.492	27975.619	od	4.5	3854.012	ev	3.5	17.9 ± 1.0	−0.34
4144.847	30637.157	ev	2.5	6517.619	od	2.5	7.6 ± 0.8	−0.93
4144.996	29735.413	od	4.5	5616.739	ev	4.5	49.1 ± 2.6	0.10
4145.486	30637.157	ev	2.5	6521.332	od	1.5	1.56 ± 0.14	−1.62
4146.232	28634.516	ev	5.5	4523.033	od	4.5	24.6 ± 1.4	−0.12
4148.162	30065.164	ev	3.5	5964.896	od	3.5	8.4 ± 0.6	−0.76
4149.143	32372.621	od	4.5	8278.054	ev	5.5	3.72 ± 0.27	−1.02
4149.781	29807.078	ev	3.5	5716.216	od	3.5	8.2 ± 0.6	−0.77
4149.966	29908.904	ev	4.5	5819.113	od	4.5	34.0 ± 2.1	−0.06
4150.404	30637.157	ev	2.5	6549.908	od	2.5	0.97 ± 0.10	−1.82
4151.970	29591.873	od	6.5	5513.709	ev	5.5	75 ± 4	0.43
4153.126	25945.396	ev	3.5	1873.934	od	3.5	7.6 ± 0.4	−0.80
4153.406	29994.041	ev	2.5	5924.204	od	1.5	2.03 ± 0.21	−1.50
4160.106	28297.473	ev	3.5	4266.397	od	3.5	3.6 ± 0.3	−1.12
4160.440	29994.041	ev	2.5	5964.896	od	3.5	0.59 ± 0.06	−2.04
4162.872	28337.814	ev	2.5	4322.708	od	2.5	1.54 ± 0.15	−1.62
4165.599	31340.393	od	6.5	7341.007	ev	5.5	90 ± 5	0.52
4165.850	32802.165	ev	5.5	8804.224	od	4.5	6.6 ± 0.7	−0.68
4166.649	28730.712	ev	3.5	4737.373	od	2.5	10.3 ± 0.6	−0.67
4167.582	29807.078	ev	3.5	5819.113	od	4.5	2.39 ± 0.14	−1.30
4169.766	29794.517	ev	3.5	5819.113	od	4.5	13.6 ± 1.0	−0.55
4169.877	28297.473	ev	3.5	4322.708	od	2.5	21.2 ± 1.1	−0.35
4171.384	29908.904	ev	4.5	5942.798	od	3.5	3.2 ± 0.4	−1.08
4172.152	26841.384	ev	4.5	2879.695	od	5.5	3.26 ± 0.19	−1.07
4174.470	28685.758	ev	2.5	4737.373	od	2.5	4.9 ± 0.3	−1.11
4175.233	29908.904	ev	4.5	5964.896	od	3.5	4.2 ± 0.3	−0.95
4176.076	27934.638	ev	4.5	3995.460	od	3.5	3.84 ± 0.26	−1.00
4179.075	31155.623	ev	6.5	7233.627	od	5.5	3.11 ± 0.22	−0.94
4185.331	27249.669	ev	2.5	3363.427	od	2.5	16.4 ± 0.9	−0.59
4187.322	28334.756	ev	4.5	4459.872	od	3.5	14.2 ± 0.8	−0.43
4189.183	29807.078	ev	3.5	5942.798	od	3.5	3.45 ± 0.22	−1.14
4189.638	31155.623	ev	6.5	7293.938	od	6.5	3.41 ± 0.18	−0.90
4192.754	29281.374	ev	2.5	5437.422	od	3.5	4.2 ± 0.3	−1.18
4193.065	29807.078	ev	3.5	5964.896	od	3.5	6.6 ± 0.6	−0.85
4193.283	32372.621	od	4.5	8531.678	ev	3.5	41.7 ± 2.4	0.04
4193.871	28297.473	ev	3.5	4459.872	od	3.5	15.6 ± 0.8	−0.48
4195.276	29794.517	ev	3.5	5964.896	od	3.5	2.80 ± 0.23	−1.23
4195.815	28337.814	ev	2.5	4511.257	od	2.5	6.8 ± 0.4	−0.97
4196.332	27187.047	ev	3.5	3363.427	od	2.5	21.6 ± 1.2	−0.34
4197.510	27812.398	ev	2.5	3995.460	od	3.5	5.8 ± 0.4	−1.03
4197.669	27811.496	ev	3.5	3995.460	od	3.5	9.1 ± 0.6	−0.72
4198.429	28334.756	ev	4.5	4523.033	od	4.5	8.2 ± 0.5	−0.66
4198.721	27975.619	od	4.5	4165.550	ev	4.5	18.0 ± 1.0	−0.32
4202.712	29438.817	ev	5.5	5651.357	od	5.5	0.57 ± 0.09	−1.74
4202.931	28297.473	ev	3.5	4511.257	od	2.5	22.0 ± 1.2	−0.33

Table 2
(Continued)

λ_{air} (Å)	E_{upper} (cm^{-1})	Parity	J_{upp}	E_{lower} (cm^{-1})	Parity	J_{low}	A-value (10^6 s^{-1})	log(gf)
4202.958	27379.949	ev	5.5	3593.882	od	4.5	10.8 ± 0.6	−0.46
4204.717	30166.057	ev	3.5	6389.942	od	4.5	2.47 ± 0.20	−1.28
4205.013	28297.473	ev	3.5	4523.033	od	4.5	0.32 ± 0.05	−2.17
4207.028	29438.817	ev	5.5	5675.763	od	4.5	0.107 ± 0.016	−2.47
4209.406	29263.338	od	5.5	5513.709	ev	5.5	7.8 ± 0.5	−0.61
4210.233	30134.910	ev	5.5	6389.942	od	4.5	1.15 ± 0.06	−1.44
4213.035	29166.597	ev	4.5	5437.422	od	3.5	4.30 ± 0.24	−0.94
4214.033	28634.516	ev	5.5	4910.963	od	5.5	11.1 ± 0.8	−0.45
4222.597	24663.053	ev	4.5	987.611	od	4.5	26.7 ± 1.4	−0.15
4223.881	27934.638	ev	4.5	4266.397	od	3.5	4.5 ± 0.3	−0.92
4227.747	29263.338	od	5.5	5616.739	ev	4.5	25.0 ± 1.3	−0.10
4228.295	30702.610	ev	4.5	7059.072	od	4.5	5.0 ± 0.3	−0.87
4230.119	27835.233	ev	1.5	4201.893	od	1.5	3.90 ± 0.24	−1.38
4230.180	31155.623	ev	6.5	7522.622	od	5.5	0.96 ± 0.15	−1.44
4231.327	30829.124	ev	3.5	7202.529	od	2.5	0.51 ± 0.04	−1.96
4232.561	29438.817	ev	5.5	5819.113	od	4.5	5.3 ± 0.3	−0.77
4233.959	28730.712	ev	3.5	5118.806	od	2.5	1.68 ± 0.15	−1.44
4234.210	27812.398	ev	2.5	4201.893	od	1.5	14.3 ± 0.9	−0.64
4234.728	30245.878	ev	4.5	6638.258	od	4.5	4.8 ± 0.3	−0.89
4236.016	28337.814	ev	2.5	4737.373	od	2.5	15.0 ± 0.8	−0.62
4236.354	32372.621	od	4.5	8774.064	ev	4.5	10.3 ± 0.9	−0.56
4238.553	27379.949	ev	5.5	3793.634	od	6.5	0.59 ± 0.07	−1.72
4239.909	27432.782	od	4.5	3854.012	ev	3.5	36.8 ± 1.9	0.00
4242.359	29281.374	ev	2.5	5716.216	od	3.5	0.60 ± 0.07	−2.01
4242.720	25945.396	ev	3.5	2382.246	od	4.5	11.9 ± 0.6	−0.59
4245.973	27811.496	ev	3.5	4266.397	od	3.5	15.4 ± 0.9	−0.48
4246.713	25681.488	ev	1.5	2140.492	od	0.5	25.6 ± 1.3	−0.56
4247.447	26900.354	ev	3.5	3363.427	od	2.5	2.07 ± 0.18	−1.35
4248.671	29043.854	od	6.5	5513.709	ev	5.5	40.3 ± 2.1	0.18
4250.692	29908.904	ev	4.5	6389.942	od	4.5	1.23 ± 0.09	−1.48
4251.855	27835.233	ev	1.5	4322.708	od	2.5	7.3 ± 0.6	−1.10
4253.362	27249.669	ev	2.5	3745.475	od	1.5	17.4 ± 0.9	−0.55
4254.000	28345.313	ev	0.5	4844.644	od	1.5	1.38 ± 0.16	−2.13
4254.728	30134.910	ev	5.5	6638.258	od	4.5	0.88 ± 0.08	−1.54
4255.358	28337.814	ev	2.5	4844.644	od	1.5	3.31 ± 0.23	−1.27
4255.782	29166.597	ev	4.5	5675.763	od	4.5	27.0 ± 1.4	−0.13
4255.989	27812.398	ev	2.5	4322.708	od	2.5	6.6 ± 0.6	−0.97
4256.152	27811.496	ev	3.5	4322.708	od	2.5	8.3 ± 0.6	−0.74
4256.702	25359.686	ev	2.5	1873.934	od	3.5	0.138 ± 0.013	−2.65
4257.119	27187.047	ev	3.5	3703.594	od	3.5	3.33 ± 0.24	−1.14
4258.394	29994.041	ev	2.5	6517.619	od	2.5	3.8 ± 0.3	−1.20
4259.068	29994.041	ev	2.5	6521.332	od	1.5	2.60 ± 0.20	−1.37
4259.594	29438.817	ev	5.5	5969.007	od	5.5	0.73 ± 0.08	−1.62
4259.744	30702.610	ev	4.5	7233.627	od	5.5	7.5 ± 0.5	−0.69
4264.368	30702.610	ev	4.5	7259.075	od	3.5	10.2 ± 0.7	−0.56
4269.176	29807.078	ev	3.5	6389.942	od	4.5	1.78 ± 0.17	−1.41
4270.184	27934.638	ev	4.5	4523.033	od	4.5	19.6 ± 1.2	−0.27
4278.859	25945.396	ev	3.5	2581.257	od	4.5	6.3 ± 0.3	−0.86
4279.941	30637.157	ev	2.5	7278.922	od	1.5	0.57 ± 0.07	−2.03
4280.136	29281.374	ev	2.5	5924.204	od	1.5	12.6 ± 0.7	−0.68
4280.987	27812.398	ev	2.5	4459.872	od	3.5	6.9 ± 0.4	−0.95
4281.153	27811.496	ev	3.5	4459.872	od	3.5	4.8 ± 0.3	−0.98
4283.546	29281.374	ev	2.5	5942.798	od	3.5	3.30 ± 0.23	−1.26
4287.144	32372.621	od	4.5	9053.629	ev	3.5	1.72 ± 0.15	−1.32
4287.606	29281.374	ev	2.5	5964.896	od	3.5	1.49 ± 0.13	−1.61
4288.663	25945.396	ev	3.5	2634.666	od	2.5	5.25 ± 0.28	−0.94
4289.447	26900.354	ev	3.5	3593.882	od	4.5	8.0 ± 0.6	−0.75
4289.932	25945.396	ev	3.5	2641.559	od	3.5	58.4 ± 3.0	0.11
4290.428	27812.398	ev	2.5	4511.257	od	2.5	1.63 ± 0.15	−1.57
4290.594	27811.496	ev	3.5	4511.257	od	2.5	1.51 ± 0.10	−1.48
4291.874	28730.712	ev	3.5	5437.422	od	3.5	0.238 ± 0.028	−2.28
4292.580	29807.078	ev	3.5	6517.619	od	2.5	8.3 ± 0.7	−0.74
4292.764	27811.496	ev	3.5	4523.033	od	4.5	6.3 ± 0.4	−0.85
4292.900	28725.148	ev	4.5	5437.422	od	3.5	1.61 ± 0.13	−1.35
4294.897	29794.517	ev	3.5	6517.619	od	2.5	1.80 ± 0.13	−1.40
4296.051	29908.904	ev	4.5	6638.258	od	4.5	5.1 ± 0.5	−0.85

Table 2
(Continued)

λ_{air} (Å)	E_{upper} (cm^{-1})	Parity	J_{upp}	E_{lower} (cm^{-1})	Parity	J_{low}	A-value (10^6 s^{-1})	log(gf)
4296.681	27432.782	od	4.5	4165.550	ev	4.5	53.2 ± 2.7	0.17
4296.779	30180.096	ev	6.5	6913.392	od	6.5	23.5 ± 1.3	−0.04
4299.087	27249.669	ev	2.5	3995.460	od	3.5	4.71 ± 0.28	−1.11
4299.357	24663.053	ev	4.5	1410.304	od	4.5	9.9 ± 0.5	−0.56
4300.328	26841.384	ev	4.5	3593.882	od	4.5	22.1 ± 1.1	−0.21
4300.863	29794.517	ev	3.5	6549.908	od	2.5	3.80 ± 0.26	−1.07
4304.717	29166.597	ev	4.5	5942.798	od	3.5	7.4 ± 0.4	−0.69
4305.140	30134.910	ev	5.5	6913.392	od	6.5	20.3 ± 1.2	−0.17
4305.605	28337.814	ev	2.5	5118.806	od	2.5	2.93 ± 0.26	−1.31
4306.726	27378.515	od	5.5	4165.550	ev	4.5	24.2 ± 1.3	−0.09
4309.580	29166.597	ev	4.5	5969.007	od	5.5	4.7 ± 0.3	−0.88
4309.735	26900.354	ev	3.5	3703.594	od	3.5	15.5 ± 1.0	−0.46
4310.696	27187.047	ev	3.5	3995.460	od	3.5	5.1 ± 0.4	−0.94
4311.585	30245.878	ev	4.5	7059.072	od	4.5	7.5 ± 0.5	−0.68
4312.853	30702.610	ev	4.5	7522.622	od	5.5	0.89 ± 0.09	−1.60
4313.099	28297.473	ev	3.5	5118.806	od	2.5	2.26 ± 0.14	−1.30
4313.592	27379.949	ev	5.5	4203.934	od	6.5	0.77 ± 0.06	−1.59
4314.932	29807.078	ev	3.5	6638.258	od	4.5	3.04 ± 0.22	−1.17
4317.273	29794.517	ev	3.5	6638.258	od	4.5	1.29 ± 0.23	−1.54
4320.719	26841.384	ev	4.5	3703.594	od	3.5	14.5 ± 0.8	−0.39
4324.785	30829.124	ev	3.5	7713.089	od	4.5	16.7 ± 1.3	−0.43
4326.479	30166.057	ev	3.5	7059.072	od	4.5	0.76 ± 0.08	−1.77
4330.441	25681.488	ev	1.5	2595.644	od	1.5	13.0 ± 0.7	−0.83
4331.757	32802.165	ev	5.5	9723.335	od	4.5	13.1 ± 0.9	−0.35
4332.319	30134.910	ev	5.5	7059.072	od	4.5	0.56 ± 0.06	−1.72
4332.472	27812.398	ev	2.5	4737.373	od	2.5	1.29 ± 0.11	−1.66
4332.641	27811.496	ev	3.5	4737.373	od	2.5	2.54 ± 0.21	−1.24
4332.703	28725.148	ev	4.5	5651.357	od	5.5	9.2 ± 0.5	−0.59
4337.291	28725.148	ev	4.5	5675.763	od	4.5	1.03 ± 0.07	−1.54
4337.387	29438.817	ev	5.5	6389.942	od	4.5	1.19 ± 0.11	−1.40
4337.594	27249.669	ev	2.5	4201.893	od	1.5	1.87 ± 0.20	−1.50
4337.773	25681.488	ev	1.5	2634.666	od	2.5	43.5 ± 2.2	−0.31
4342.135	27934.638	ev	4.5	4910.963	od	5.5	1.74 ± 0.19	−1.31
4343.866	28730.712	ev	3.5	5716.216	od	3.5	2.42 ± 0.19	−1.26
4344.917	28725.148	ev	4.5	5716.216	od	3.5	1.18 ± 0.13	−1.48
4345.453	30065.164	ev	3.5	7059.072	od	4.5	2.70 ± 0.22	−1.21
4348.585	30702.610	ev	4.5	7713.089	od	4.5	1.25 ± 0.10	−1.45
4349.768	27249.669	ev	2.5	4266.397	od	3.5	11.1 ± 0.6	−0.73
4349.789	28634.516	ev	5.5	5651.357	od	5.5	14.0 ± 0.9	−0.32
4352.707	27812.398	ev	2.5	4844.644	od	1.5	32.9 ± 1.9	−0.25
4355.923	30829.124	ev	3.5	7878.328	od	3.5	0.60 ± 0.07	−1.86
4356.744	30180.096	ev	6.5	7233.627	od	5.5	1.77 ± 0.18	−1.15
4359.064	31738.484	ev	5.5	8804.224	od	4.5	5.5 ± 0.9	−0.72
4360.169	29449.778	ev	1.5	6521.332	od	1.5	9.5 ± 0.7	−0.97
4361.652	27187.047	ev	3.5	4266.397	od	3.5	4.9 ± 0.3	−0.95
4364.653	26900.354	ev	3.5	3995.460	od	3.5	29.5 ± 1.9	−0.17
4365.341	30134.910	ev	5.5	7233.627	od	5.5	0.62 ± 0.10	−1.67
4365.511	28337.814	ev	2.5	5437.422	od	3.5	2.56 ± 0.19	−1.36
4366.094	28334.756	ev	4.5	5437.422	od	3.5	0.229 ± 0.028	−2.18
4368.226	30180.096	ev	6.5	7293.938	od	6.5	3.40 ± 0.23	−0.87
4369.235	29892.677	od	3.5	7011.804	ev	4.5	5.6 ± 0.4	−0.89
4372.394	27187.047	ev	3.5	4322.708	od	2.5	2.82 ± 0.16	−1.19
4373.215	28297.473	ev	3.5	5437.422	od	3.5	1.78 ± 0.14	−1.39
4373.814	27379.949	ev	5.5	4523.033	od	4.5	9.7 ± 0.6	−0.48
4375.170	29908.904	ev	4.5	7059.072	od	4.5	2.89 ± 0.21	−1.08
4375.919	26841.384	ev	4.5	3995.460	od	3.5	14.9 ± 0.8	−0.37
4376.868	30134.910	ev	5.5	7293.938	od	6.5	0.74 ± 0.06	−1.59
4380.053	27835.233	ev	1.5	5010.870	od	2.5	8.6 ± 0.8	−1.01
4381.080	30637.157	ev	2.5	7818.147	od	1.5	2.63 ± 0.23	−1.34
4381.773	28634.516	ev	5.5	5819.113	od	4.5	4.6 ± 0.3	−0.80
4382.165	28327.071	od	5.5	5513.709	ev	5.5	39.2 ± 2.2	0.13
4384.439	27812.398	ev	2.5	5010.870	od	2.5	0.66 ± 0.05	−1.94
4386.366	29994.041	ev	2.5	7202.529	od	2.5	4.8 ± 0.3	−1.08
4386.696	27249.669	ev	2.5	4459.872	od	3.5	14.6 ± 0.8	−0.60
4386.827	24663.053	ev	4.5	1873.934	od	3.5	14.3 ± 0.7	−0.38

Table 2
(Continued)

λ_{air} (Å)	E_{upper} (cm^{-1})	Parity	J_{upp}	E_{lower} (cm^{-1})	Parity	J_{low}	A-value (10^6 s^{-1})	log(gf)
4387.059	28730.712	ev	3.5	5942.798	od	3.5	4.4 ± 0.4	−0.99
4388.005	29750.547	od	5.5	6967.547	ev	6.5	11.8 ± 0.6	−0.39
4390.760	32492.038	ev	5.5	9723.335	od	4.5	0.42 ± 0.05	−1.84
4391.317	28730.712	ev	3.5	5964.896	od	3.5	1.70 ± 0.14	−1.41
4391.659	25359.686	ev	2.5	2595.644	od	1.5	52.9 ± 2.7	−0.04
4393.184	28725.148	ev	4.5	5969.007	od	5.5	9.3 ± 0.6	−0.57
4396.609	27249.669	ev	2.5	4511.257	od	2.5	2.33 ± 0.16	−1.39
4397.183	29794.517	ev	3.5	7059.072	od	4.5	0.70 ± 0.07	−1.79
4397.276	29994.041	ev	2.5	7259.075	od	3.5	2.87 ± 0.21	−1.30
4398.783	27187.047	ev	3.5	4459.872	od	3.5	7.5 ± 0.5	−0.76
4399.200	25359.686	ev	2.5	2634.666	od	2.5	21.1 ± 1.1	−0.44
4399.474	29735.413	od	4.5	7011.804	ev	4.5	0.94 ± 0.10	−1.56
4399.542	30245.878	ev	4.5	7522.622	od	5.5	1.72 ± 0.13	−1.30
4400.535	25359.686	ev	2.5	2641.559	od	3.5	3.18 ± 0.22	−1.26
4400.865	27835.233	ev	1.5	5118.806	od	2.5	9.6 ± 0.7	−0.95
4405.293	27812.398	ev	2.5	5118.806	od	2.5	1.96 ± 0.19	−1.47
4405.468	27811.496	ev	3.5	5118.806	od	2.5	3.9 ± 0.4	−1.04
4407.272	28334.756	ev	4.5	5651.357	od	5.5	6.6 ± 0.4	−0.71
4412.020	28334.756	ev	4.5	5675.763	od	4.5	4.9 ± 0.3	−0.84
4416.900	26900.354	ev	3.5	4266.397	od	3.5	7.4 ± 0.5	−0.76
4418.780	29591.873	od	6.5	6967.547	ev	6.5	45.1 ± 2.5	0.27
4427.069	25945.396	ev	3.5	3363.427	od	2.5	9.9 ± 0.6	−0.63
4427.208	28297.473	ev	3.5	5716.216	od	3.5	0.63 ± 0.10	−1.83
4427.916	26900.354	ev	3.5	4322.708	od	2.5	16.7 ± 1.1	−0.41
4428.438	26841.384	ev	4.5	4266.397	od	3.5	9.0 ± 0.5	−0.58
4432.912	27835.233	ev	1.5	5283.029	od	0.5	5.3 ± 0.3	−1.20
4433.738	29807.078	ev	3.5	7259.075	od	3.5	1.84 ± 0.13	−1.36
4436.209	29794.517	ev	3.5	7259.075	od	3.5	1.70 ± 0.13	−1.40
4440.110	28334.756	ev	4.5	5819.113	od	4.5	0.44 ± 0.05	−1.89
4443.747	27934.638	ev	4.5	5437.422	od	3.5	6.3 ± 0.4	−0.73
4449.330	27379.949	ev	5.5	4910.963	od	5.5	31.0 ± 1.8	0.04
4449.633	30637.157	ev	2.5	8169.698	od	1.5	10.2 ± 1.0	−0.74
4450.732	27975.619	od	4.5	5513.709	ev	5.5	23.0 ± 1.2	−0.17
4450.854	30637.157	ev	2.5	8175.863	od	2.5	2.17 ± 0.23	−1.41
4452.504	30166.057	ev	3.5	7713.089	od	4.5	1.23 ± 0.18	−1.53
4453.158	27187.047	ev	3.5	4737.373	od	2.5	1.94 ± 0.19	−1.34
4454.982	26900.354	ev	3.5	4459.872	od	3.5	3.16 ± 0.24	−1.12
4457.768	30829.124	ev	3.5	8402.668	od	3.5	4.3 ± 0.4	−0.99
4458.831	28345.313	ev	0.5	5924.204	od	1.5	1.49 ± 0.17	−2.05
4459.077	30166.057	ev	3.5	7746.185	od	2.5	1.08 ± 0.10	−1.59
4460.207	26268.203	od	3.5	3854.012	ev	3.5	80 ± 4	0.28
4461.133	29750.547	od	5.5	7341.007	ev	5.5	23.1 ± 1.3	−0.08
4462.032	27249.669	ev	2.5	4844.644	od	1.5	0.338 ± 0.028	−2.22
4465.437	29449.778	ev	1.5	7061.838	od	0.5	5.8 ± 0.4	−1.16
4466.720	26841.384	ev	4.5	4459.872	od	3.5	0.48 ± 0.05	−1.84
4467.073	29438.817	ev	5.5	7059.072	od	4.5	1.05 ± 0.15	−1.42
4468.025	27812.398	ev	2.5	5437.422	od	3.5	0.50 ± 0.06	−2.04
4469.508	30245.878	ev	4.5	7878.328	od	3.5	0.44 ± 0.04	−1.88
4471.241	27975.619	od	4.5	5616.739	ev	4.5	56.0 ± 2.9	0.23
4472.082	28297.473	ev	3.5	5942.798	od	3.5	0.81 ± 0.08	−1.71
4472.602	30065.164	ev	3.5	7713.089	od	4.5	6.3 ± 0.6	−0.82
4472.715	25945.396	ev	3.5	3593.882	od	4.5	10.6 ± 0.6	−0.60
4479.235	30065.164	ev	3.5	7746.185	od	2.5	7.3 ± 0.5	−0.75
4479.361	26841.384	ev	4.5	4523.033	od	4.5	12.0 ± 0.7	−0.44
4479.419	25681.488	ev	1.5	3363.427	od	2.5	9.8 ± 0.7	−0.93
4483.059	30702.610	ev	4.5	8402.668	od	3.5	0.84 ± 0.11	−1.60
4483.893	29263.338	od	5.5	6967.547	ev	6.5	34.9 ± 1.8	0.10
4485.515	30166.057	ev	3.5	7878.328	od	3.5	9.3 ± 0.8	−0.65
4486.909	24663.053	ev	4.5	2382.246	od	4.5	22.0 ± 1.2	−0.18
4492.947	29591.873	od	6.5	7341.007	ev	5.5	1.99 ± 0.13	−1.07
4493.554	29994.041	ev	2.5	7746.185	od	2.5	0.59 ± 0.07	−1.97
4494.217	28634.516	ev	5.5	6389.942	od	4.5	5.9 ± 0.5	−0.67
4495.385	27249.669	ev	2.5	5010.870	od	2.5	7.1 ± 0.5	−0.89
4496.256	30637.157	ev	2.5	8402.668	od	3.5	8.0 ± 0.7	−0.84
4499.507	27934.638	ev	4.5	5716.216	od	3.5	0.52 ± 0.06	−1.80
4508.079	27187.047	ev	3.5	5010.870	od	2.5	3.39 ± 0.27	−1.08

Table 2
(Continued)

λ_{air} (Å)	E_{upper} (cm^{-1})	Parity	J_{upp}	E_{lower} (cm^{-1})	Parity	J_{low}	A-value (10^6 s^{-1})	log(gf)
4508.721	25681.488	ev	1.5	3508.470	od	0.5	2.10 ± 0.16	−1.59
4509.255	29892.677	od	3.5	7722.285	ev	2.5	3.48 ± 0.24	−1.07
4510.763	26900.354	ev	3.5	4737.373	od	2.5	0.41 ± 0.05	−2.00
4520.404	29994.041	ev	2.5	7878.328	od	3.5	1.96 ± 0.26	−1.44
4523.075	26268.203	od	3.5	4165.550	ev	4.5	34.2 ± 1.8	−0.08
4524.849	29807.078	ev	3.5	7713.089	od	4.5	1.11 ± 0.09	−1.56
4527.348	24663.053	ev	4.5	2581.257	od	4.5	21.0 ± 1.2	−0.19
4527.423	29794.517	ev	3.5	7713.089	od	4.5	4.6 ± 0.5	−0.95
4527.953	29281.374	ev	2.5	7202.529	od	2.5	2.07 ± 0.16	−1.42
4528.473	29043.854	od	6.5	6967.547	ev	6.5	45.2 ± 2.4	0.29
4534.219	29794.517	ev	3.5	7746.185	od	2.5	2.58 ± 0.30	−1.20
4537.874	29908.904	ev	4.5	7878.328	od	3.5	4.0 ± 0.4	−0.90
4539.745	24663.053	ev	4.5	2641.559	od	3.5	26.7 ± 1.4	−0.08
4544.953	25359.686	ev	2.5	3363.427	od	2.5	8.8 ± 0.5	−0.79
4545.867	27934.638	ev	4.5	5942.798	od	3.5	1.89 ± 0.17	−1.23
4551.291	27934.638	ev	4.5	5969.007	od	5.5	12.2 ± 0.8	−0.42
4554.545	25945.396	ev	3.5	3995.460	od	3.5	1.86 ± 0.11	−1.33
4555.608	28334.756	ev	4.5	6389.942	od	4.5	1.07 ± 0.09	−1.48
4558.068	29166.597	ev	4.5	7233.627	od	5.5	0.49 ± 0.06	−1.82
4558.598	26841.384	ev	4.5	4910.963	od	5.5	3.38 ± 0.21	−0.98
4559.243	29449.778	ev	1.5	7522.458	od	0.5	1.15 ± 0.19	−1.84
4560.280	29263.338	od	5.5	7341.007	ev	5.5	40.7 ± 2.1	0.18
4560.958	27432.782	od	4.5	5513.709	ev	5.5	17.8 ± 1.0	−0.26
4562.359	25766.355	od	4.5	3854.012	ev	3.5	51.8 ± 2.6	0.21
4568.036	30166.057	ev	3.5	8280.946	od	2.5	0.40 ± 0.04	−2.00
4569.670	32802.165	ev	5.5	10924.876	od	4.5	5.8 ± 0.5	−0.66
4572.278	27378.515	od	5.5	5513.709	ev	5.5	43.7 ± 2.2	0.22
4576.799	30245.878	ev	4.5	8402.668	od	3.5	0.80 ± 0.08	−1.60
4582.050	29994.041	ev	2.5	8175.863	od	2.5	0.52 ± 0.06	−2.00
4582.406	28337.814	ev	2.5	6521.332	od	1.5	6.0 ± 0.4	−0.95
4582.499	27432.782	od	4.5	5616.739	ev	4.5	14.1 ± 0.8	−0.35
4588.416	28337.814	ev	2.5	6549.908	od	2.5	2.93 ± 0.21	−1.26
4589.374	24663.053	ev	4.5	2879.695	od	5.5	0.336 ± 0.027	−1.97
4591.116	30702.610	ev	4.5	8927.514	od	5.5	12.2 ± 1.0	−0.41
4593.926	27378.515	od	5.5	5616.739	ev	4.5	31.1 ± 1.6	0.07
4596.928	28297.473	ev	3.5	6549.908	od	2.5	1.16 ± 0.12	−1.53
4601.374	32372.621	od	4.5	10646.070	ev	5.5	4.9 ± 0.4	−0.81
4604.226	29994.041	ev	2.5	8280.946	od	2.5	2.45 ± 0.30	−1.33
4606.400	29043.854	od	6.5	7341.007	ev	5.5	19.5 ± 1.0	−0.06
4613.033	28730.712	ev	3.5	7059.072	od	4.5	2.34 ± 0.22	−1.22
4613.528	32372.621	od	4.5	10703.305	ev	4.5	0.92 ± 0.13	−1.53
4618.930	29166.597	ev	4.5	7522.622	od	5.5	0.99 ± 0.09	−1.50
4621.743	30829.124	ev	3.5	9198.326	od	3.5	0.86 ± 0.11	−1.66
4623.477	25945.396	ev	3.5	4322.708	od	2.5	0.53 ± 0.03	−1.87
4625.290	25359.686	ev	2.5	3745.475	od	1.5	0.41 ± 0.03	−2.10
4628.161	25766.355	od	4.5	4165.550	ev	4.5	42.5 ± 2.2	0.14
4630.183	29994.041	ev	2.5	8402.668	od	3.5	0.14 ± 0.03	−2.55
4633.601	28634.516	ev	5.5	7059.072	od	4.5	1.58 ± 0.23	−1.21
4636.741	27379.949	ev	5.5	5819.113	od	4.5	0.66 ± 0.07	−1.59
4640.214	27934.638	ev	4.5	6389.942	od	4.5	0.341 ± 0.027	−1.96
4643.774	28730.712	ev	3.5	7202.529	od	2.5	1.03 ± 0.10	−1.57
4644.216	29807.078	ev	3.5	8280.946	od	2.5	5.1 ± 0.4	−0.88
4647.422	27187.047	ev	3.5	5675.763	od	4.5	2.04 ± 0.18	−1.28
4648.513	29908.904	ev	4.5	8402.668	od	3.5	0.51 ± 0.05	−1.78
4654.278	25681.488	ev	1.5	4201.893	od	1.5	8.7 ± 0.6	−0.95
4656.003	28730.712	ev	3.5	7259.075	od	3.5	2.9 ± 0.4	−1.12
4656.178	27187.047	ev	3.5	5716.216	od	3.5	0.85 ± 0.10	−1.66
4657.210	28725.148	ev	4.5	7259.075	od	3.5	1.59 ± 0.18	−1.29
4657.828	29281.374	ev	2.5	7818.147	od	1.5	2.22 ± 0.17	−1.36
4659.101	29735.413	od	4.5	8278.054	ev	5.5	0.25 ± 0.03	−2.10
4659.938	29166.597	ev	4.5	7713.089	od	4.5	2.16 ± 0.22	−1.15
4664.149	25945.396	ev	3.5	4511.257	od	2.5	0.41 ± 0.07	−1.97
4666.713	25945.396	ev	3.5	4523.033	od	4.5	1.00 ± 0.15	−1.58
4666.889	27811.496	ev	3.5	6389.942	od	4.5	0.41 ± 0.05	−1.97
4670.098	28685.758	ev	2.5	7278.922	od	1.5	3.4 ± 0.3	−1.18
4670.627	29807.078	ev	3.5	8402.668	od	3.5	0.67 ± 0.09	−1.75

Table 2
(Continued)

λ_{air} (Å)	E_{upper} (cm^{-1})	Parity	J_{upp}	E_{lower} (cm^{-1})	Parity	J_{low}	A-value (10^6 s^{-1})	log(gf)
4670.725	26841.384	ev	4.5	5437.422	od	3.5	3.08 ± 0.19	−1.00
4671.395	28634.516	ev	5.5	7233.627	od	5.5	0.76 ± 0.13	−1.53
4678.600	27187.047	ev	3.5	5819.113	od	4.5	1.17 ± 0.11	−1.51
4679.412	25359.686	ev	2.5	3995.460	od	3.5	0.57 ± 0.08	−1.95
4680.119	29892.677	od	3.5	8531.678	ev	3.5	12.6 ± 1.0	−0.48
4680.442	28327.071	od	5.5	6967.547	ev	6.5	1.57 ± 0.10	−1.21
4680.986	32372.621	od	4.5	11015.579	ev	3.5	5.4 ± 0.4	−0.75
4684.598	28634.516	ev	5.5	7293.938	od	6.5	10.3 ± 0.8	−0.39
4686.770	30134.910	ev	5.5	8804.224	od	4.5	3.38 ± 0.28	−0.87
4687.608	29750.547	od	5.5	8423.672	ev	6.5	0.85 ± 0.08	−1.48
4689.479	30245.878	ev	4.5	8927.514	od	5.5	2.47 ± 0.17	−1.09
4690.160	28327.071	od	5.5	7011.804	ev	4.5	1.48 ± 0.11	−1.23
4690.479	29591.873	od	6.5	8278.054	ev	5.5	2.15 ± 0.16	−1.00
4692.009	27249.669	ev	2.5	5942.798	od	3.5	2.27 ± 0.21	−1.35
4694.320	27934.638	ev	4.5	6638.258	od	4.5	0.47 ± 0.05	−1.81
4694.872	27811.496	ev	3.5	6517.619	od	2.5	2.91 ± 0.22	−1.11
4695.375	29994.041	ev	2.5	8702.444	od	1.5	1.20 ± 0.09	−1.62
4698.886	28334.756	ev	4.5	7059.072	od	4.5	0.36 ± 0.05	−1.93
4702.002	27811.496	ev	3.5	6549.908	od	2.5	2.34 ± 0.18	−1.21
4707.932	28327.071	od	5.5	7092.265	ev	5.5	1.81 ± 0.17	−1.14
4710.198	26900.354	ev	3.5	5675.763	od	4.5	0.61 ± 0.08	−1.79
4714.017	30134.910	ev	5.5	8927.514	od	5.5	11.7 ± 0.7	−0.33
4714.831	29735.413	od	4.5	8531.678	ev	3.5	7.5 ± 0.5	−0.60
4717.881	26841.384	ev	4.5	5651.357	od	5.5	2.15 ± 0.25	−1.14
4719.193	26900.354	ev	3.5	5716.216	od	3.5	0.29 ± 0.04	−2.12
4722.293	25681.488	ev	1.5	4511.257	od	2.5	2.55 ± 0.17	−1.47
4722.746	29591.873	od	6.5	8423.672	ev	6.5	0.98 ± 0.07	−1.34
4723.321	26841.384	ev	4.5	5675.763	od	4.5	1.25 ± 0.08	−1.38
4730.101	28337.814	ev	2.5	7202.529	od	2.5	6.4 ± 0.4	−0.89
4732.366	26841.384	ev	4.5	5716.216	od	3.5	0.83 ± 0.07	−1.55
4733.835	29892.677	od	3.5	8774.064	ev	4.5	1.77 ± 0.17	−1.32
4737.271	29892.677	od	3.5	8789.380	ev	2.5	29.0 ± 1.8	−0.11
4739.147	28297.473	ev	3.5	7202.529	od	2.5	3.11 ± 0.24	−1.08
4742.227	26900.354	ev	3.5	5819.113	od	4.5	0.68 ± 0.07	−1.74
4744.944	24663.053	ev	4.5	3593.882	od	4.5	1.90 ± 0.12	−1.19
4747.260	28337.814	ev	2.5	7278.922	od	1.5	0.80 ± 0.10	−1.79
4749.234	30829.124	ev	3.5	9778.986	od	2.5	2.05 ± 0.20	−1.26
4757.841	28725.148	ev	4.5	7713.089	od	4.5	5.7 ± 0.4	−0.71
4759.927	29807.078	ev	3.5	8804.224	od	4.5	2.63 ± 0.17	−1.14
4762.840	27379.949	ev	5.5	6389.942	od	4.5	0.194 ± 0.021	−2.10
4763.735	28327.071	od	5.5	7341.007	ev	5.5	0.145 ± 0.027	−2.23
4763.912	29263.338	od	5.5	8278.054	ev	5.5	3.53 ± 0.23	−0.84
4768.791	27975.619	od	4.5	7011.804	ev	4.5	4.7 ± 0.4	−0.80
4769.782	24663.053	ev	4.5	3703.594	od	3.5	0.245 ± 0.025	−2.08
4773.941	28396.150	od	2.5	7454.951	ev	1.5	20.0 ± 1.2	−0.39
4775.463	25945.396	ev	3.5	5010.870	od	2.5	1.20 ± 0.19	−1.49
4787.165	27975.619	od	4.5	7092.265	ev	5.5	1.37 ± 0.15	−1.33
4788.230	29281.374	ev	2.5	8402.668	od	3.5	1.73 ± 0.19	−1.45
4789.682	26841.384	ev	4.5	5969.007	od	5.5	0.93 ± 0.13	−1.49
4792.944	30637.157	ev	2.5	9778.986	od	2.5	0.87 ± 0.13	−1.75
4795.184	25359.686	ev	2.5	4511.257	od	2.5	1.89 ± 0.22	−1.41
4795.554	28725.148	ev	4.5	7878.328	od	3.5	2.13 ± 0.25	−1.13
4797.343	29892.677	od	3.5	9053.629	ev	3.5	0.49 ± 0.05	−1.87
4797.426	29735.413	od	4.5	8896.729	ev	5.5	1.08 ± 0.07	−1.43
4797.850	25681.488	ev	1.5	4844.644	od	1.5	0.27 ± 0.03	−2.43
4804.633	28685.758	ev	2.5	7878.328	od	3.5	0.76 ± 0.08	−1.80
4812.505	27835.233	ev	1.5	7061.838	od	0.5	1.97 ± 0.19	−1.56
4835.674	28396.150	od	2.5	7722.285	ev	2.5	5.8 ± 0.4	−0.92
4847.914	28334.756	ev	4.5	7713.089	od	4.5	5.0 ± 0.5	−0.75
4848.263	29043.854	od	6.5	8423.672	ev	6.5	0.97 ± 0.07	−1.32
4850.902	27811.496	ev	3.5	7202.529	od	2.5	1.52 ± 0.15	−1.37
4858.729	29892.677	od	3.5	9316.912	ev	3.5	4.9 ± 0.4	−0.86
4861.821	25681.488	ev	1.5	5118.806	od	2.5	0.42 ± 0.06	−2.23
4863.673	28730.712	ev	3.5	8175.863	od	2.5	0.95 ± 0.11	−1.57
4863.838	30829.124	ev	3.5	10274.971	od	3.5	1.80 ± 0.24	−1.29
4873.999	29438.817	ev	5.5	8927.514	od	5.5	4.7 ± 0.5	−0.69

Table 2
(Continued)

λ_{air} (Å)	E_{upper} (cm^{-1})	Parity	J_{upp}	E_{lower} (cm^{-1})	Parity	J_{low}	A-value (10^6 s^{-1})	log(gf)
4874.211	26900.354	ev	3.5	6389.942	od	4.5	0.25 ± 0.05	−2.14
4882.463	32802.165	ev	5.5	12326.417	od	6.5	35.8 ± 2.4	0.19
4887.074	28334.756	ev	4.5	7878.328	od	3.5	0.31 ± 0.05	−1.96
4890.351	30166.057	ev	3.5	9723.335	od	4.5	1.71 ± 0.16	−1.31
4895.558	27432.782	od	4.5	7011.804	ev	4.5	0.72 ± 0.04	−1.59
4895.998	28297.473	ev	3.5	7878.328	od	3.5	1.30 ± 0.10	−1.43
4896.152	29735.413	od	4.5	9316.912	ev	3.5	0.34 ± 0.05	−1.91
4897.959	27378.515	od	5.5	6967.547	ev	6.5	0.292 ± 0.028	−1.90
4901.396	24663.053	ev	4.5	4266.397	od	3.5	0.54 ± 0.08	−1.71
4903.700	30166.057	ev	3.5	9778.986	od	2.5	1.62 ± 0.19	−1.33
4912.919	25359.686	ev	2.5	5010.870	od	2.5	0.20 ± 0.03	−2.35
4914.607	30065.164	ev	3.5	9723.335	od	4.5	1.59 ± 0.18	−1.34
4914.924	27432.782	od	4.5	7092.265	ev	5.5	4.3 ± 0.3	−0.81
4917.939	28730.712	ev	3.5	8402.668	od	3.5	0.38 ± 0.04	−1.95
4928.072	27378.515	od	5.5	7092.265	ev	5.5	1.15 ± 0.08	−1.30
4932.112	25945.396	ev	3.5	5675.763	od	4.5	0.30 ± 0.04	−2.06
4946.624	30245.878	ev	4.5	10035.711	od	5.5	2.00 ± 0.19	−1.14
4952.134	30829.124	ev	3.5	10641.442	od	2.5	0.37 ± 0.06	−1.96
4962.103	29043.854	od	6.5	8896.729	ev	5.5	0.39 ± 0.04	−1.69
4967.241	25945.396	ev	3.5	5819.113	od	4.5	0.29 ± 0.04	−2.07
4968.395	28297.473	ev	3.5	8175.863	od	2.5	1.30 ± 0.12	−1.41
4977.201	27379.949	ev	5.5	7293.938	od	6.5	2.26 ± 0.27	−1.00
4984.433	28337.814	ev	2.5	8280.946	od	2.5	4.2 ± 0.4	−1.02
4991.014	31340.393	od	6.5	11309.972	ev	7.5	4.0 ± 0.3	−0.68
4994.478	28297.473	ev	3.5	8280.946	od	2.5	2.7 ± 0.3	−1.09
4994.727	29794.517	ev	3.5	9778.986	od	2.5	5.4 ± 0.5	−0.79
4997.956	25945.396	ev	3.5	5942.798	od	3.5	0.148 ± 0.018	−2.35
5000.958	27249.669	ev	2.5	7259.075	od	3.5	0.85 ± 0.08	−1.72
5002.779	28685.758	ev	2.5	8702.444	od	1.5	6.6 ± 0.6	−0.83
5011.759	28396.150	od	2.5	8448.641	ev	2.5	14.3 ± 1.0	−0.49
5015.138	27812.398	ev	2.5	7878.328	od	3.5	0.67 ± 0.06	−1.82
5015.365	27811.496	ev	3.5	7878.328	od	3.5	0.41 ± 0.05	−1.91
5018.448	28725.148	ev	4.5	8804.224	od	4.5	0.30 ± 0.05	−1.95
5022.652	30829.124	ev	3.5	10924.876	od	4.5	0.63 ± 0.10	−1.72
5022.867	28327.071	od	5.5	8423.672	ev	6.5	9.2 ± 0.7	−0.38
5027.339	31340.393	od	6.5	11454.701	ev	6.5	3.2 ± 0.5	−0.77
5028.263	31340.393	od	6.5	11458.353	ev	5.5	2.68 ± 0.26	−0.85
5037.800	27975.619	od	4.5	8131.217	ev	4.5	7.0 ± 0.6	−0.57
5039.273	30637.157	ev	2.5	10798.555	od	2.5	1.43 ± 0.14	−1.49
5044.023	29591.873	od	6.5	9771.956	ev	7.5	13.5 ± 1.0	−0.14
5049.701	28725.148	ev	4.5	8927.514	od	5.5	0.37 ± 0.04	−1.85
5072.924	28634.516	ev	5.5	8927.514	od	5.5	1.56 ± 0.20	−1.14
5075.355	27975.619	od	4.5	8278.054	ev	5.5	11.5 ± 0.8	−0.35
5083.279	27379.949	ev	5.5	7713.089	od	4.5	0.50 ± 0.06	−1.64
5085.216	27835.233	ev	1.5	8175.863	od	2.5	0.52 ± 0.06	−2.10
5089.487	28345.313	ev	0.5	8702.444	od	1.5	1.62 ± 0.21	−1.90
5105.227	26841.384	ev	4.5	7259.075	od	3.5	1.22 ± 0.11	−1.32
5106.217	29892.677	od	3.5	10314.162	ev	4.5	0.57 ± 0.08	−1.75
5112.543	27835.233	ev	1.5	8280.946	od	2.5	0.94 ± 0.12	−1.83
5117.946	29591.873	od	6.5	10058.226	ev	6.5	2.8 ± 0.3	−0.81
5118.349	29807.078	ev	3.5	10274.971	od	3.5	0.96 ± 0.11	−1.52
5141.737	29166.597	ev	4.5	9723.335	od	4.5	0.40 ± 0.03	−1.80
5144.844	27249.669	ev	2.5	7818.147	od	1.5	1.12 ± 0.16	−1.58
5145.156	28327.071	od	5.5	8896.729	ev	5.5	1.93 ± 0.22	−1.04
5146.910	30065.164	ev	3.5	10641.442	od	2.5	1.17 ± 0.13	−1.43
5147.565	29735.413	od	4.5	10314.162	ev	4.5	12.5 ± 0.9	−0.30
5150.860	27811.496	ev	3.5	8402.668	od	3.5	0.58 ± 0.07	−1.73
5163.547	29449.778	ev	1.5	10088.640	od	1.5	0.47 ± 0.09	−2.12
5187.458	29043.854	od	6.5	9771.956	ev	7.5	26.2 ± 1.8	0.17
5191.633	26268.203	od	3.5	7011.804	ev	4.5	7.8 ± 0.6	−0.60
5192.092	32372.621	od	4.5	13117.922	ev	4.5	1.55 ± 0.24	−1.20
5208.108	29994.041	ev	2.5	10798.555	od	2.5	0.42 ± 0.08	−1.99
5210.339	26900.354	ev	3.5	7713.089	od	4.5	2.64 ± 0.30	−1.07
5216.701	25681.488	ev	1.5	6517.619	od	2.5	1.17 ± 0.13	−1.72
5217.711	25681.488	ev	1.5	6521.332	od	1.5	1.07 ± 0.15	−1.76
5225.505	25681.488	ev	1.5	6549.908	od	2.5	2.6 ± 0.3	−1.38

Table 2
(Continued)

λ_{air} (Å)	E_{upper} (cm^{-1})	Parity	J_{upp}	E_{lower} (cm^{-1})	Parity	J_{low}	A-value (10^6 s^{-1})	log(gf)
5226.402	26841.384	ev	4.5	7713.089	od	4.5	1.08 ± 0.16	−1.35
5232.918	29750.547	od	5.5	10646.070	ev	5.5	10.0 ± 0.9	−0.31
5234.019	27378.515	od	5.5	8278.054	ev	5.5	3.3 ± 0.3	−0.79
5237.067	29735.413	od	4.5	10646.070	ev	5.5	5.8 ± 0.5	−0.62
5241.333	27249.669	ev	2.5	8175.863	od	2.5	0.73 ± 0.08	−1.75
5241.777	29892.677	od	3.5	10820.486	ev	2.5	2.52 ± 0.26	−1.08
5252.817	29735.413	od	4.5	10703.305	ev	4.5	1.72 ± 0.15	−1.15
5262.938	29449.778	ev	1.5	10454.272	od	1.5	1.18 ± 0.25	−1.71
5265.506	29994.041	ev	2.5	11007.799	od	1.5	0.26 ± 0.05	−2.20
5265.677	29043.854	od	6.5	10058.226	ev	6.5	10.0 ± 0.7	−0.23
5274.229	27378.515	od	5.5	8423.672	ev	6.5	26.8 ± 1.6	0.13
5276.457	24663.053	ev	4.5	5716.216	od	3.5	0.102 ± 0.010	−2.37
5283.386	27975.619	od	4.5	9053.629	ev	3.5	1.06 ± 0.09	−1.35
5294.855	29750.547	od	5.5	10869.541	ev	4.5	0.43 ± 0.05	−1.66
5295.155	30829.124	ev	3.5	11949.189	od	3.5	0.53 ± 0.09	−1.75
5304.408	27249.669	ev	2.5	8402.668	od	3.5	0.52 ± 0.07	−1.88
5327.492	29449.778	ev	1.5	10684.441	od	0.5	1.00 ± 0.15	−1.77
5330.556	25766.355	od	4.5	7011.804	ev	4.5	9.3 ± 0.7	−0.40
5350.020	25945.396	ev	3.5	7259.075	od	3.5	0.127 ± 0.017	−2.36
5353.524	25766.355	od	4.5	7092.265	ev	5.5	28.8 ± 1.7	0.09
5369.864	29263.338	od	5.5	10646.070	ev	5.5	0.20 ± 0.04	−1.98
5383.812	30829.124	ev	3.5	12260.088	od	3.5	0.40 ± 0.06	−1.86
5386.773	28337.814	ev	2.5	9778.986	od	2.5	7.5 ± 0.6	−0.71
5390.523	26268.203	od	3.5	7722.285	ev	2.5	0.35 ± 0.04	−1.91
5393.392	27432.782	od	4.5	8896.729	ev	5.5	19.9 ± 1.3	−0.06
5398.508	28297.473	ev	3.5	9778.986	od	2.5	1.60 ± 0.13	−1.25
5409.229	27378.515	od	5.5	8896.729	ev	5.5	9.8 ± 0.7	−0.29
5413.051	29794.517	ev	3.5	11325.781	od	2.5	0.51 ± 0.06	−1.75
5433.927	29043.854	od	6.5	10646.070	ev	5.5	0.53 ± 0.04	−1.48
5435.105	29263.338	od	5.5	10869.541	ev	4.5	0.361 ± 0.029	−1.72
5459.193	31340.393	od	6.5	13027.758	ev	6.5	7.5 ± 0.9	−0.33
5464.203	29750.547	od	5.5	11454.701	ev	6.5	5.8 ± 0.6	−0.50
5468.371	29591.873	od	6.5	11309.972	ev	7.5	13.4 ± 1.1	−0.07
5505.941	25359.686	ev	2.5	7202.529	od	2.5	0.54 ± 0.05	−1.84
5512.064	26268.203	od	3.5	8131.217	ev	4.5	11.3 ± 1.0	−0.39
5513.118	29591.873	od	6.5	11458.353	ev	5.5	1.47 ± 0.19	−1.03
5518.489	27432.782	od	4.5	9316.912	ev	3.5	4.9 ± 0.4	−0.65
5524.450	32372.621	od	4.5	14276.298	ev	5.5	2.44 ± 0.27	−0.95
5547.079	28297.473	ev	3.5	10274.971	od	3.5	0.194 ± 0.027	−2.15
5550.033	28327.071	od	5.5	10314.162	ev	4.5	2.00 ± 0.20	−0.96
5561.445	29735.413	od	4.5	11759.467	ev	5.5	2.83 ± 0.26	−0.88
5610.253	26268.203	od	3.5	8448.641	ev	2.5	5.9 ± 0.5	−0.65
5613.694	29263.338	od	5.5	11454.701	ev	6.5	4.1 ± 0.4	−0.64
5637.359	29043.854	od	6.5	11309.972	ev	7.5	3.6 ± 0.3	−0.62
5654.219	28327.071	od	5.5	10646.070	ev	5.5	0.248 ± 0.028	−1.85
5659.517	25945.396	ev	3.5	8280.946	od	2.5	0.262 ± 0.027	−2.00
5660.476	27975.619	od	4.5	10314.162	ev	4.5	0.51 ± 0.04	−1.61
5667.960	29735.413	od	4.5	12097.276	ev	3.5	1.56 ± 0.16	−1.12
5683.745	29043.854	od	6.5	11454.701	ev	6.5	2.03 ± 0.16	−0.86
5684.925	29043.854	od	6.5	11458.353	ev	5.5	0.77 ± 0.08	−1.28
5733.693	29892.677	od	3.5	12456.746	ev	3.5	1.59 ± 0.17	−1.20
5768.891	27975.619	od	4.5	10646.070	ev	5.5	6.0 ± 0.5	−0.52
5771.975	27378.515	od	5.5	10058.226	ev	6.5	1.38 ± 0.12	−1.08
5788.007	27975.619	od	4.5	10703.305	ev	4.5	0.85 ± 0.12	−1.37
5822.479	27811.496	ev	3.5	10641.442	od	2.5	0.29 ± 0.05	−1.92
5832.290	25945.396	ev	3.5	8804.224	od	4.5	0.54 ± 0.06	−1.65
5839.973	27432.782	od	4.5	10314.162	ev	4.5	0.23 ± 0.05	−1.92
5842.096	29438.817	ev	5.5	12326.417	od	6.5	0.58 ± 0.06	−1.45
5858.546	27378.515	od	5.5	10314.162	ev	4.5	1.08 ± 0.19	−1.18
5895.679	28297.473	ev	3.5	11340.598	od	3.5	0.44 ± 0.06	−1.73
5898.083	24663.053	ev	4.5	7713.089	od	4.5	0.53 ± 0.06	−1.56
5959.688	29892.677	od	3.5	13117.922	ev	4.5	4.8 ± 0.5	−0.69
5968.060	31155.623	ev	6.5	14404.400	od	7.5	1.33 ± 0.13	−1.00
5975.818	27432.782	od	4.5	10703.305	ev	4.5	6.6 ± 0.6	−0.45
5995.265	27378.515	od	5.5	10703.305	ev	4.5	1.62 ± 0.17	−0.98
5995.448	29892.677	od	3.5	13217.976	ev	3.5	2.01 ± 0.19	−1.06

Table 2
(Continued)

λ_{air} (Å)	E_{upper} (cm^{-1})	Parity	J_{upp}	E_{lower} (cm^{-1})	Parity	J_{low}	A-value (10^6 s^{-1})	log(gf)
6013.568	29892.677	od	3.5	13268.218	ev	2.5	1.72 ± 0.23	−1.13
6034.205	28327.071	od	5.5	11759.467	ev	5.5	3.5 ± 0.4	−0.64
6035.476	29591.873	od	6.5	13027.758	ev	6.5	2.37 ± 0.25	−0.74
6043.373	26268.203	od	3.5	9725.733	ev	3.5	7.5 ± 0.8	−0.48
6069.634	27811.496	ev	3.5	11340.598	od	3.5	0.76 ± 0.11	−1.47
6101.243	28334.756	ev	4.5	11949.189	od	3.5	0.29 ± 0.04	−1.79
6108.747	29892.677	od	3.5	13527.239	ev	4.5	4.2 ± 0.5	−0.73
6183.954	25945.396	ev	3.5	9778.986	od	2.5	0.89 ± 0.10	−1.39
6225.397	31340.393	od	6.5	15281.602	ev	6.5	0.49 ± 0.05	−1.40
6232.448	25766.355	od	4.5	9725.733	ev	3.5	2.2 ± 0.3	−0.89
6272.026	28396.150	od	2.5	12456.746	ev	3.5	11.1 ± 1.1	−0.40
6296.145	27975.619	od	4.5	12097.276	ev	3.5	0.66 ± 0.08	−1.41
6371.109	28396.150	od	2.5	12704.634	ev	1.5	6.6 ± 0.7	−0.62
6428.509	27811.496	ev	3.5	12260.088	od	3.5	0.35 ± 0.05	−1.77
6441.986	27975.619	od	4.5	12456.746	ev	3.5	0.42 ± 0.05	−1.58
6449.503	26841.384	ev	4.5	11340.598	od	3.5	0.126 ± 0.016	−2.10
6466.888	29735.413	od	4.5	14276.298	ev	5.5	3.6 ± 0.5	−0.65
6507.163	29750.547	od	5.5	14387.112	ev	4.5	1.39 ± 0.15	−0.97
6608.464	28396.150	od	2.5	13268.218	ev	2.5	0.52 ± 0.07	−1.69
6609.726	29750.547	od	5.5	14625.503	ev	5.5	0.69 ± 0.08	−1.27
6616.346	29735.413	od	4.5	14625.503	ev	5.5	0.85 ± 0.10	−1.25
6706.051	29735.413	od	4.5	14827.623	ev	3.5	1.92 ± 0.24	−0.89
6720.280	29263.338	od	5.5	14387.112	ev	4.5	1.52 ± 0.13	−0.91
6829.583	28297.473	ev	3.5	13659.329	od	4.5	0.134 ± 0.022	−2.13
6829.727	29263.338	od	5.5	14625.503	ev	5.5	1.68 ± 0.15	−0.85
6905.307	30637.157	ev	2.5	16159.536	od	3.5	0.84 ± 0.11	−1.44
6919.282	27975.619	od	4.5	13527.239	ev	4.5	1.41 ± 0.14	−0.99
6960.365	29892.677	od	3.5	15529.576	ev	2.5	0.19 ± 0.04	−1.95
6983.822	27432.782	od	4.5	13117.922	ev	4.5	0.88 ± 0.12	−1.19
7025.915	29794.517	ev	3.5	15565.420	od	2.5	0.45 ± 0.07	−1.57
7061.753	29750.547	od	5.5	15593.660	ev	6.5	8.1 ± 0.9	−0.14
7075.546	29263.338	od	5.5	15134.048	ev	4.5	0.27 ± 0.04	−1.62
7086.353	31340.393	od	6.5	17232.652	ev	7.5	12.6 ± 1.4	0.12
7142.824	25945.396	ev	3.5	11949.189	od	3.5	0.128 ± 0.018	−2.11
7238.371	26268.203	od	3.5	12456.746	ev	3.5	1.96 ± 0.20	−0.91
7275.857	29892.677	od	3.5	16152.377	ev	3.5	0.133 ± 0.022	−2.07
7349.808	29794.517	ev	3.5	16192.466	od	4.5	0.16 ± 0.03	−1.98
7360.097	29735.413	od	4.5	16152.377	ev	3.5	0.51 ± 0.07	−1.38
7439.467	29892.677	od	3.5	16454.555	ev	2.5	0.33 ± 0.05	−1.66
7486.722	27835.233	ev	1.5	14481.930	od	2.5	0.33 ± 0.06	−1.96
7496.946	27432.782	od	4.5	14097.689	ev	3.5	0.70 ± 0.08	−1.23
7577.678	28327.071	od	5.5	15134.048	ev	4.5	0.43 ± 0.05	−1.35
7583.580	25945.396	ev	3.5	12762.641	od	4.5	0.065 ± 0.011	−2.35
7584.818	27432.782	od	4.5	14252.178	ev	3.5	0.39 ± 0.05	−1.47
7596.363	28396.150	od	2.5	15235.579	ev	1.5	0.66 ± 0.10	−1.47
7660.593	26268.203	od	3.5	13217.976	ev	3.5	0.27 ± 0.03	−1.72
7690.200	26268.203	od	3.5	13268.218	ev	2.5	0.63 ± 0.07	−1.35
7711.746	30134.910	ev	5.5	17171.245	od	5.5	0.29 ± 0.04	−1.51
7851.195	28327.071	od	5.5	15593.660	ev	6.5	1.99 ± 0.25	−0.66
7939.063	26268.203	od	3.5	13675.722	ev	2.5	0.58 ± 0.07	−1.36
8068.524	32372.621	od	4.5	19982.187	ev	4.5	1.45 ± 0.24	−0.85
8088.901	29591.873	od	6.5	17232.652	ev	7.5	1.47 ± 0.19	−0.69
8137.064	25945.396	ev	3.5	13659.329	od	4.5	0.139 ± 0.020	−1.96
8233.415	28334.756	ev	4.5	16192.466	od	4.5	0.18 ± 0.03	−1.73
8693.756	29892.677	od	3.5	18393.327	ev	3.5	0.61 ± 0.11	−1.26
8777.180	31340.393	od	6.5	19950.340	ev	6.5	0.81 ± 0.12	−0.88
8926.473	25681.488	ev	1.5	14481.930	od	2.5	0.34 ± 0.05	−1.78
9014.550	27249.669	ev	2.5	16159.536	od	3.5	0.099 ± 0.017	−2.14
9050.375	29750.547	od	5.5	18704.313	ev	5.5	0.37 ± 0.06	−1.27
9602.004	29892.677	od	3.5	19481.040	ev	4.5	0.21 ± 0.03	−1.64
10433.058	27975.619	od	4.5	18393.327	ev	3.5	0.102 ± 0.018	−1.78
10783.013	27975.619	od	4.5	18704.313	ev	5.5	0.33 ± 0.05	−1.24

(This table is also available in a machine-readable form in the online journal.)

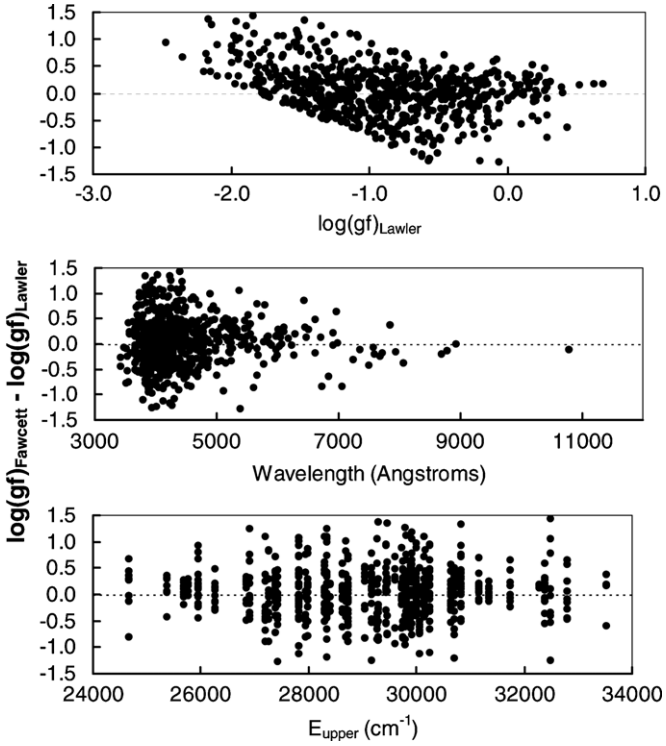

Figure 2. Comparison of theoretical Ce II transition probabilities from Fawcett (1990) to our transition probabilities as function of our transition probability or log(*gf*), wavelength, and upper level energy.

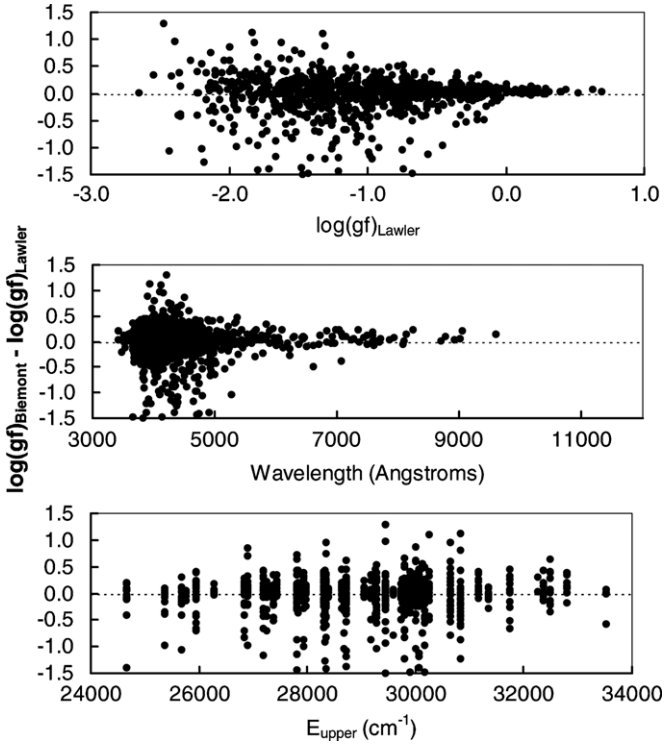

Figure 3. Comparison of Ce II transition probabilities recently downloaded from the DREAM database (Biémont & Quinet 2005) to our transition probabilities as function of our transition probability or log(*gf*), wavelength, and upper level energy.

A more substantive question arises about the accuracy of the new experimental results. The agreement between our new experimental results and the various large-scale theoretical and

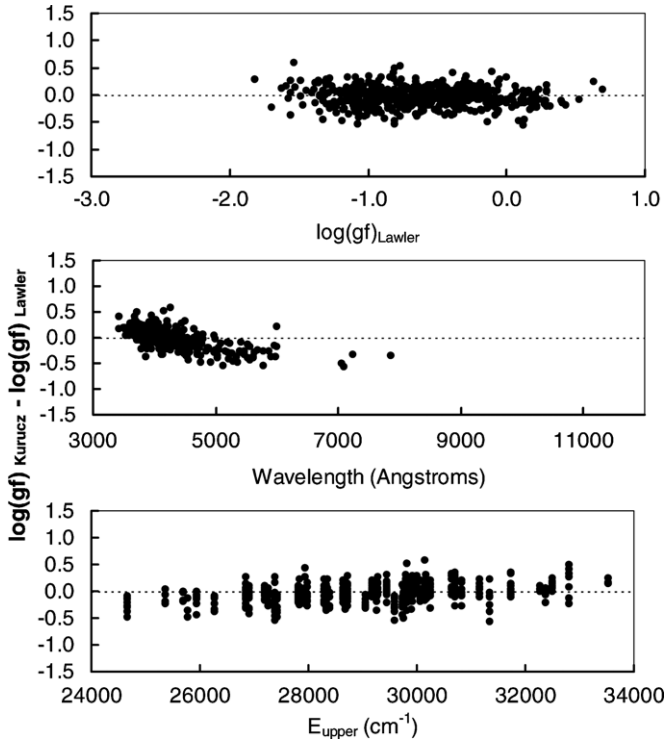

Figure 4. Comparison of semiempirical Ce II transition probabilities recently downloaded from the Kurucz. database (Kurucz 1998) to our transition probabilities as function of our transition probability or log(*gf*), wavelength, and upper level energy.

semiempirical data sets is not impressive in any of the above comparisons. One might ask if our experimental error bars are reasonable. This question was recently addressed in a detailed comparison (Lawler et al. 2008a) between Sm II transition probabilities measured as part of this program (Lawler et al. 2006), and independent transition probability measurements from Rehse et al. (2006). Figure 5 shows comparisons of these two experimental data sets for Sm II that were published almost simultaneously. A total of 347 lines in common are included. Lines in common from two levels reported by Rehse et al. and identified as problematic (S. D. Rosner 2007, private communication) are omitted. The two experiments that produced these data sets on Sm II are quite different. A detailed discussion of the relative strengths, weaknesses, and possible systematic errors of both experiments is available (Lawler et al. 2008a). The agreement between these two experimental data sets is much better than the agreement of either with theoretical results.

3. SOLAR AND STELLAR CERIUM ABUNDANCES

We used the Ce II transition probabilities to determine new Ce abundances in the solar photosphere and five very metal-poor ([Fe/H] < -2), "*r*-process" *n*-capture-rich giant stars. Our procedures followed those used in previous papers of this series; see Den Hartog et al. (2006); Lawler et al. (2006, 2007, 2008b), and references therein.

3.1. Line Selection

Cool stars exhibit a rich Ce II spectrum. For example, the solar photospheric line compendium of Moore et al. 1966 lists nearly 200 lines of this species. Therefore identification of transitions suitable for abundance analysis was a straightforward task. We

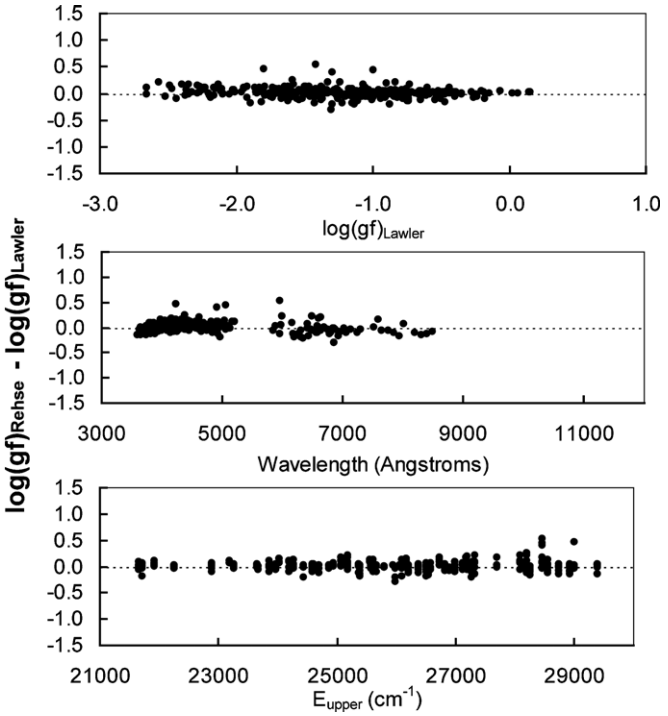

Figure 5. Comparison of experimental Sm II transition probabilities from Rehse et al. (2006) to our transition probabilities as functions of our transition probability or log(*gf*), wavelength, and upper level energy. This plot illustrates the level of agreement now achieved between modern, but rather different, experimental techniques.

began by computing relative line strength factors for all 921 Ce II lines of Table 2. As discussed in Lawler et al. (2008b and references therein), the relative absorption strengths of weak-to-moderate lines within a given species are proportional to their transition probabilities modified by their Boltzmann excitation factors. For a line on the linear part of the curve-of-growth this relationship is

$$\log(\mathrm{RW}) = \log(\mathrm{EW}/\lambda) = \mathrm{constant} + \log(\mathrm{g}f) - \theta\chi$$

where RW is the reduced width, EW is the equivalent width (mÅ), *gf* is the oscillator strength, χ is the excitation energy, and $\theta = 5040/\mathrm{T}$ is the inverse temperature.

The relative strengths of lines of different species also depend on their elemental abundances and Saha ionization equilibrium factors. However, Ce, like all REs, has a low first ionization potential: 5.539 eV (Grigoriev & Melikhov 1997). They all are completely ionized in the stellar photospheres of the Sun and stars of our sample; corrections for their other ionization state populations are negligible. Thus the relative strength factor (STR) of a line can be written as

$$\mathrm{STR} \equiv \log(\varepsilon \mathrm{g}f) - \theta\chi,$$

where ε is the elemental abundance. In Figure 6 we plot these relative strength factors as a function of wavelength for Gd II lines (Den Hartog et al. 2006) and Ce II lines (this paper). For these computations we used solar abundances: log ε(Gd) = +1.11 (Den Hartog et al. 2006) and log ε(Ce) = +1.55, which is close to the recommended meteoritic Ce abundance of log ε(Ce) = +1.58 (Lodders (2003). We also adopted $\theta = 1.0$ for this exercise, roughly the average value of the Sun and the metal-poor giants considered here (since most detectable Gd II and Ce II transitions in these stars have $\chi < 1$ eV, the exact value of θ is not important in this exercise).

As in our previous studies, we have drawn horizontal lines in Figure 6 to indicate approximate STR values for "strong" and "barely detectable" lines. These were defined by Lawler et al. (2006) for Sm II, who used the Delbouille et al. (1973) solar photospheric spectrum to estimate the EWs of the weakest lines that could routinely be employed in abundance analyses. The EW limit is ≈1.5 mÅ in the spectral region $\lambda \sim 4500$ Å, or log(RW) ≈ −6.5. For such Ce II lines, STR ≈ −0.6. That EW and thus STR limit applies also to Gd II and Ce II lines, as shown in both panels of Figure 6 with horizontal dotted lines. A minimum STR value for relatively strong lines was estimated by Lawler et al. (2006), defining it to be a factor of 20 larger than the line detection limit value, or STR = −0.6 + 1.3 = +0.7. We have indicated this "strong-line" limit in Figure 6 with dashed horizontal lines.

Figure 6 displays STR values only in the wavelength range 3000 Å $\leqslant \lambda \leqslant$ 7000 Å even though our transition probability data extend to nearly 11000 Å (1.1 μm). Nearly all Gd II and Ce II lines beyond 7000 Å are undetectably weak in the stars of interest here, having solar relative strengths STR < −1.0. Clearly the "strong" lines of Gd II, Ce II, and nearly all RE ions occur in the blue and near-UV spectral regions ($\lambda < 4500$ Å), which we emphasize with vertical lines drawn at 4000 Å in the figure. Fortunately, about 70 strong Ce II lines (STR > +0.7) lie longward of 4000 Å, and thus are easily accessible to ground-based spectroscopy in a (relatively) un-congested spectral domain. No strong Gd II lines are so fortuitously located.

The Ce II STR values were used to trim the original set of 921 transitions (Table 2) to about 620, by discarding those lines weaker than STR < –0.6. We then searched through this list to identify potentially useful Ce II lines for abundance analyses. We inspected these lines in the solar photospheric center-of-disk spectrum of Delbouille et al. (1973) and in our spectrum of the *r*-process-rich metal-poor giant star CS 31082–001 ([Fe/H] = −2.9, [Eu/Fe] = +1.7, Hill et al. 2002). These spectra, aided by the Moore et al. (1966) solar line identifications and the comprehensive Kurucz (1998) atomic and molecular line lists, showed that the vast majority of candidate Ce II transitions are too weak and/or too blended to be of use in the Sun and stars of interest here. This process produced a final set of about 60 lines for more detailed study.

3.2. The Solar Photospheric Cerium Abundance

We computed synthetic spectra for the Ce II lines as in previous papers of this series. Briefly, we started with atomic and molecular line lists in small (4–6 Å) wavelength regions, from Kurucz's (1998) line database, supplemented in a few cases by Moore et al.'s (1966) solar identifications. We adopted *gf*-values from laboratory studies for these ionized *n*-capture element species: Y, Hannaford et al. (1982); Zr, Malcheva et al. (2006); La, Lawler et al. (2001a); Ce, this study; Nd, Den Hartog et al. (2003); Sm, Lawler et al. (2006); Eu, Lawler et al. (2001b); Gd, Den Hartog et al. (2006); Tb, Lawler et al. (2001c); Dy, Wickliffe et al. (2000); Ho, Lawler et al. (2004); Er, Lawler et al. (2008b); and Hf, Lawler et al. (2007). The Ce II transitions were treated as single features, since their hyperfine and isotopic substructures are very small.

We adopted the Holweger & Müller (1974) empirical model photosphere for most of the solar computations. Standard solar abundances were taken from recent reviews (e.g., Grevesse &

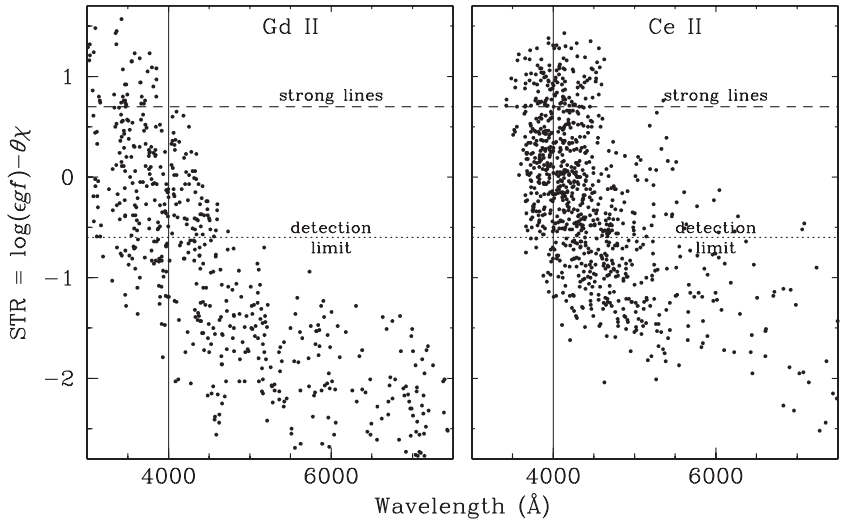

Figure 6. Relative transition strength factors, STR ≡ log(εgf)–$\theta\chi$, for Gd II (Den Hartog et al. 2006) and Ce II (this study). Definitions of "detection limit" and "strong lines" are given in the text. For display purposes the long-wavelength limit has been set to 7000 Å. Lines longward of this limit are too weak to be detected in any of the stars of this study. The short-wavelength limit of 3000 Å is defined by the Earth atmospheric transmission cutoff. All Ce II lines of this study are longward of this limit.

Sauval 2002; Lodders 2003; Grevesse et al. 2007), modified for some elements to include recent updates for the *n*-capture elements (given in the papers cited above). We input the solar model, abundance set, and line lists into the current version of the LTE line analysis code MOOG (Sneden 1973) to generate synthetic spectra. These were matched to the observed solar spectrum (Delbouille et al. 1973) after application of empirical Gaussian broadening functions to account for solar macroturbulence and spectrograph instrumental profile.

We computed multiple trial synthetic spectra for each line region. The oscillator strengths for atomic lines other than the *n*-capture species listed above were adjusted to fit the observed solar spectrum. The C, N, and O abundances were varied to match observed CH, CN, NH, and OH line strengths. For absorption features without plausible identifications, we arbitrarily attributed them to Fe I with excitation potentials χ = 3.5 eV and *gf*-values adjusted to fit the solar spectrum. In cases where line contamination was a significant part of the overall absorption at the Ce II wavelength, the line was discarded for the solar analysis but kept for possible use with the metal-poor giants. After iterating the line list data, final syntheses of 45 Ce II lines were retained for the solar analysis. Individual line abundances are listed in Table 3, along with their excitation energies and *gf*-values. A straight mean abundance is log ε(Ce) = 1.61 ± 0.01 (σ = 0.06).

For internal (line-to-line) errors, we estimate line profile fitting uncertainties to be ±0.02 dex, contamination by other (non-Ce) features to be ±0.02 dex, and log(*gf*) uncertainties for the Ce II transitions (see Table 2) are ±0.03. Adding these uncertainties in quadrature yields an estimated total internal uncertainty per transition of ±0.05 dex, which is close to the observed σ = 0.06. With solar abundance information from 45 Ce II lines, the mean standard deviation of 0.01 suggests that internal uncertainties are very small contributors to the overall error budget. Scale (external) errors can be due to atomic data uncertainties beyond *gf* errors, model atmosphere choices, and analysis technique. Since Ce exists almost exclusively as Ce II in these stars, only the Ce II partition function (which enters directly into the Boltzmann equations for our transitions) could contribute to abundance scale uncertainties. Our spectral synthesis code uses Irwin's (1981) partition function polynomial fits to the atomic energy level data available at that time. We re-calculated Ce II partition functions with current energy level information (Martin et al. 2000), but found negligible changes from the Irwin computations in the temperature domain of interest for this study. Finally, in low-metallicity stars, Rayleigh scattering becomes an important continuous opacity source in the blue-UV spectral regions, and radiative transfer source functions can depart somewhat from the Planck function assumed in our calculations. In Sneden et al. (2009) we discuss experiments with more proper accounting for continuum scattering, showing that it produces only small effects for the stars of our sample, and affects most RE elements in a nearly equal fashion, leaving abundance ratios virtually unchanged.

As in Lawler et al. (2007), we repeated some of the abundance computations using the Kurucz (1998) and Grevesse & Sauval (1999) models, finding average abundance shifts of –0.02 dex compared to those done with the Holweger & Müller (1974) model. Finally, we emphasize that our analysis is a standard LTE one with a pure Planck source function. Departures from LTE in the ionization equilibrium cannot affect our Ce II analysis because Ce is already completely ionized. The existence of many low excitation energy levels with this ion increases the likelihood of collisional dominance in their populations. Comments are included in the companion paper (Sneden et al. 2009) on the effect of inclusion of scattering in the continuum source function, but the effect is extremely small for the Sun (and weak for the *r*-process-rich stars). Combining line-to-line scatter uncertainties (±0.01 from the standard deviation of the mean, Table 3) with scale uncertainties, we recommend log $\varepsilon(\mathrm{Ce})_{\mathrm{Sun}}$ = +1.61 ± 0.03. This value is in excellent agreement with the recommended meteoritic abundance of Lodders (2003): log $\varepsilon(\mathrm{Ce})_{\mathrm{met}}$ = +1.61 ± 0.02.

Palmeri et al. (2000) published the most recent Ce abundance study of the solar photosphere. Analyzing the EWs of 26 lines, they derived log $\varepsilon(\mathrm{Ce})_{\mathrm{Sun}}$ = +1.63 ± 0.04 from one set of transition probability calculations, and +1.70 ± 0.04 from a different set. We repeated these abundance computations with their EWs, the final recommended log(*gf*) values from their web site, and our line analysis code MOOG (Sneden 1973), obtaining

Table 3
Cerium Abundances from Individual Lines in the Sun and the *r*-Process-Rich Metal-poor Giant Stars

λ (Å)	E. P. (eV)	log(gf)	log ε Sun	log ε BD +17°3248	log ε CS 22892	log ε CS 31082	log ε HD 115444	log ε HD 221170
3534.045	0.521	−0.14	1.70	−0.05	−0.44	−0.31	...	−0.35
3539.079	0.320	−0.27	...	−0.10	−0.47	...	...	−0.43
3659.225	0.175	−0.67	1.63	−0.15	−0.45	−0.29	...	−0.41
3659.970	0.175	−0.73	1.63	...	...	...	...	...
3912.420	0.295	−0.25	1.60	−0.16	−0.48	...	...	−0.44
3942.151	0.000	−0.22	1.52	−0.16	−0.47	−0.29	−1.15	−0.41
3942.745	0.857	0.69	1.50	−0.21	−0.52	−0.36	−1.15	−0.56
3953.652	0.495	−0.64	1.57	...	...	...	...	...
3980.890	0.708	−0.21	1.70	−0.13	...	...	...	...
3993.819	0.909	0.29	1.64	0.02	...	−0.24	...	...
3999.237	0.295	0.06	1.60	−0.13	−0.51	−0.31	−1.13	−0.46
4042.581	0.495	0.00	1.60	−0.02	−0.45	−0.29	−1.02	−0.41
4053.503	0.000	−0.61	1.60	−0.08	−0.45	−0.26	−1.05	−0.41
4068.836	0.703	−0.17	1.55	−0.03	...	...	...	...
4072.918	0.327	−0.64	1.61	0.00	...	−0.22	...	−0.41
4073.474	0.477	0.21	1.59	−0.10	−0.45	−0.30	−1.07	−0.43
4075.700	0.700	0.23	1.60	−0.12	−0.48	−0.31	−1.14	−0.41
4083.222	0.700	0.27	1.78	−0.08	−0.45	−0.33	−1.05	−0.41
4117.288	0.739	−0.45	1.61	...	...	−0.31	...	...
4118.143	0.696	0.13	...	−0.08	−0.43	−0.27	−0.97	−0.38
4120.827	0.320	−0.37	1.70	−0.08	−0.30	−0.22	−1.00	−0.37
4127.364	0.683	0.31	1.60	−0.08	−0.47	−0.31	−1.05	−0.44
4137.645	0.516	0.40	1.75	−0.10	−0.45	−0.28	−1.05	−0.38
4142.397	0.696	0.22	...	−0.07	...	...	...	...
4144.996	0.696	0.10	1.65	−0.14	−0.47	−0.26	−0.95	−0.38
4146.232	0.560	−0.12	...	−0.10	−0.47	−0.26	−0.90	...
4222.597	0.122	−0.15	1.58	−0.11	−0.44	−0.28	−1.07	−0.45
4337.773	0.326	−0.31	1.61	...	...	...	...	...
4349.768	0.529	−0.73	...	...	...	...	...	...
4349.789	0.700	−0.32	1.60	−0.18	−0.50	−0.29	...	−0.45
4364.653	0.495	−0.17	...	−0.17	−0.42	−0.35	−1.20	−0.49
4382.165	0.683	0.13	1.55	−0.15	...	−0.28	...	...
4399.200	0.326	−0.44	1.60	−0.11	−0.50	−0.26	...	−0.38
4418.780	0.863	0.27	1.65	−0.14	...	−0.26	−1.10	−0.38
4449.330	0.608	0.04	1.63	−0.18	−0.53	−0.31	−1.15	−0.45
4486.909	0.295	−0.18	1.61	−0.12	−0.50	−0.32	−1.08	−0.46
4523.075	0.516	−0.08	1.61	−0.04	−0.50	...	...	...
4560.280	0.909	0.18	1.65	−0.18	−0.45	−0.28	−1.07	−0.43
4560.958	0.683	−0.26	1.61	−0.12	−0.45	−0.28	−1.07	−0.41
4562.359	0.477	0.21	1.63	−0.11	−0.40	−0.26	−1.07	−0.41
4572.278	0.683	0.22	1.62	−0.08	...	−0.27	−1.04	−0.41
4582.499	0.696	−0.35	1.55	−0.07	...	−0.30	−1.07	−0.38
4593.926	0.696	0.07	1.65	−0.13	−0.45	−0.27	−1.02	−0.41
4628.161	0.516	0.14	1.57	−0.09	−0.37	−0.26	−1.05	−0.41
4847.914	0.956	−0.75	1.52	...	...	...	...	...
5044.023	1.211	−0.14	...	...	...	...	...	−0.41
5187.458	1.211	0.17	1.59	...	...	−0.31	...	−0.44
5274.229	1.044	0.13	...	−0.21	−0.40	−0.31	...	−0.46
5330.556	0.869	−0.40	1.70	...	...	−0.31	...	−0.48
5393.392	1.102	−0.06	1.55	...	−0.53	−0.31	...	−0.46
5768.891	1.319	−0.52	1.63	...	...	...	...	...
5975.818	1.326	−0.45	1.55	...	...	...	...	...
6043.373	1.205	−0.48	1.64	...	...	...	...	...
Mean			1.61	−0.11	−0.46	−0.29	−1.06	−0.42
Unc.			0.01	0.01	0.01	0.01	0.01	0.01
σ			0.06	0.05	0.05	0.03	0.07	0.04
number of lines			45	40	32	38	26	37

$\log \varepsilon(\mathrm{Ce})_{\mathrm{Sun}} = +1.67 \pm 0.04$ ($\sigma = 0.14$). Finally, we substituted their log(*gf*) values for the ones of the present study for our preferred transitions (Table 3), finding $\log \varepsilon(\mathrm{Ce})_{\mathrm{Sun}} = +1.59 \pm 0.02$ ($\sigma = 0.10$). All of these computations are consistent with the overall scale agreement between the Palmeri et al. transition probabilities and those of the present study that was discussed in Section 2.5.

3.3. Cerium Abundances in Five r-Process-Rich Low-Metallicity Stars

The spectra of several very metal-poor, *r*-process-rich giant stars were also analyzed to determine their Ce abundances: BD+17°3248 ([Fe/H] = −2.1, [Eu/Fe] = +0.9, Cowan et al. 2002); CS 22892–052 ([Fe/H] = −3.1, [Eu/Fe] = +1.5, Sneden

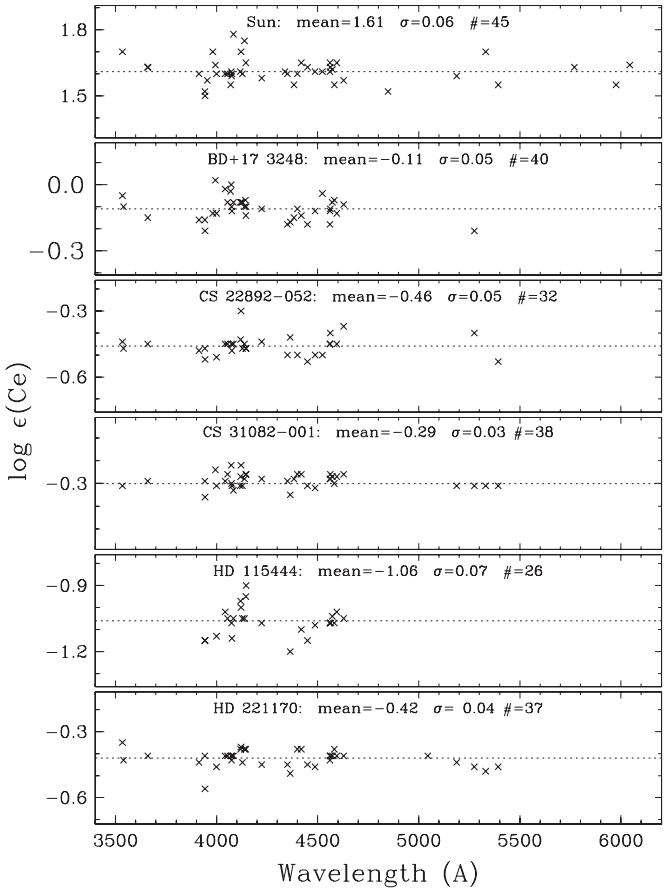

Figure 7. Abundances of individual Ce II lines for all program stars, plotted as a function of wavelength. For each star, a dotted line is drawn at the mean abundance. The mean abundances, sample standard deviation σ, and the number of lines used in the analyses are given in the legends of each figure panel.

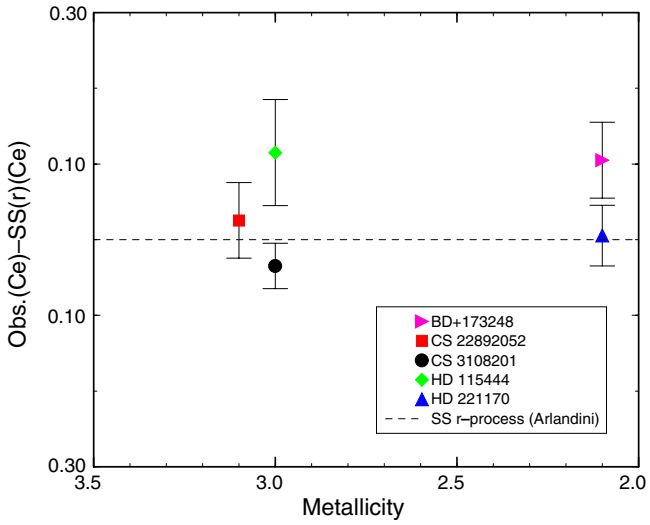

Figure 8. Comparison of the newly determined Ce abundances in five *r*-process-rich stars to the solar system *r*-process only value (Arlandini et al. 1999). For each star the abundances have been normalized at Eu. The dashed line indicates a perfect agreement between the stellar and solar system *r*-only values for Ce. The error bars are the sigma values listed for each star in Table 3.

(A color version of this figure is available in the online journal.)

et al. 2003b); CS 31082–001 ([Fe/H] = −2.9, [Eu/Fe] = +1.7, Hill et al. 2002); HD 115444 ([Fe/H] = −2.9, [Eu/Fe] = +0.8, Westin et al. 2000); and HD 221170 ([Fe/H] = −2.2, [Eu/Fe] = +0.8, Ivans et al. 2006). We employed the same analytical methods for these stars as was done for the solar photosphere. The abundances from individual lines are listed in Table 3 and displayed in Figure 7. The average abundances, mean and sample standard deviations, and number of lines are also recorded at the bottom of Table 3 and in Figure 7. The line-to-line scatters are all small, σ = 0.03–0.07, with no obvious trends of abundances as functions of wavelength, log(*gf*), or excitation potential. The line-to-line scatters for individual stars approximately anti-correlate with their Ce II line strengths. We derived the smallest scatter (σ = 0.03) for CS 31082–001, which has the strongest lines, and the largest (σ = 0.07) for HD 115444, with mostly very weak lines.

4. DISCUSSION AND CONCLUSIONS

We compare the newly derived Ce abundances among the five *r*-rich stars in Figure 8. The differences between the observed Ce abundances for each star—BD+17°3248, CS 22892–052, CS 31082–001, HD 115444, and HD 221170—and the solar system *r*-process only value (Arlandini et al. 1999) are illustrated in the figure. In all cases, the abundances have been normalized with respect to the Eu abundances. (These abundances have also been newly redetermined for those five stars and are reported in the companion paper; Sneden et al. 2009.) The corresponding error bars are those given for log ε(Ce) in Table 3. As is clear from the figure, the Ce abundances in all five *r*-rich stars are in general agreement with a solar system *r*-only value and there is little scatter among the stars – with the largest deviations from the solar *r*-process value (indicated by a dashed line) of approximately 0.1 dex. (A value of zero would thus indicate a perfect agreement with that prediction of the solar system *r*-only values.) The two stars deviating the most from the solar system *r*-process values are HD 115444 and BD 17°3248. The increased precision of our new Ce abundance determinations suggests that the error limits are typically less than 0.1 dex. Thus, it is possible that there might be some small *s*-process contamination to the Ce abundances in those two stars. (Ce is a predominantly *s*-process element, 81%, in solar system material.) If, however, this slight *s*-process contribution is due to Galactic *s*-process nucleosynthesis, we would expect to see an increasing trend in Ce abundance as a function of metallicity. Previous studies (see Burris et al. 2000 and Simmerer et al. 2004) found evidence of Galactic *s*-process nucleosynthesis at metallicities less than −2.0.

We see in Figure 8 that (somewhat surprisingly) there is no metallicity effect on the agreement between the Ce stellar and solar system *r*-process only ratios. There is an almost perfect agreement with the *r*-process only value for Ce in CS 22892–052 at [Fe/H] = −3.1 and in HD 221170 at [Fe/H] = −2.1. Since Ce is produced predominantly in the *s*-process in solar system material (see e.g., Simmerer et al. 2004), it might be expected that there would be some rise in the Ce abundance at metallicities near -2. While BD+17°3248 does show a rise at that point, there is no clear overall trend, at least for this sample of only five *r*-rich stars. Thus, there may be something specific to these two stars that would indicate Ce abundances slightly larger than, but still roughly in agreement with, the predicted *r*-process only ratios. Studies of possible small *s*-process contributions to other *s*-process-dominant RE elements, such as Ba, in these five stars studied here are included in Sneden et al. (2009).

This consistency between stellar and solar-system *r*-process-only values for RE elements is not surprising and has been reported previously for each of these stars: BD+17°3248 (Cowan

et al. 2002), CS 22892–052 (Sneden et al. 2004), CS 31082–001 (Hill et al. 2002), HD 115444 (Westin et al. 2000) and HD 221170 (Ivans et al. 2006). However, in the past there has been considerably more star-to-star scatter in individual elements, including Ce (see Figure 10 in Lawler et al. 2008b). This scatter has now been dramatically reduced for Ce with much smaller error bars than previously possible, as a result of the new atomic physics data presented in this paper. Further discussion and analyses of other RE elements, based upon new atomic data, can be found in the companion paper Sneden et al. (2009).

This work has been supported by the National Science Foundations through grants AST-0506324 to JEL & EDH, AST-0607708 to CS, and AST-0707447 to J.J.C. J.E.L. is a guest observer at the NSO on Kitt Peak, AZ.

APPENDIX

This work on Ce II, as indicated in the Introduction, completes a multiyear effort to improve laboratory spectroscopic data for RE ions and to apply these data in abundance studies. This appendix is a summary of lab data from the project including transition probabilities, isotopic shifts, hfs constants, and complete isotopic and hfs line component patterns. References are included to published data tables as well as some new MR tables. A few of our early papers did not include MR tables of transition probability data, and we have since had numerous requests for such MR tables. In other cases we published only isotope shifts and/or hfs constants without realizing that many astronomers would prefer complete isotopic and/or hyperfine line component patterns. We are here providing such tables.

We also wish to correct a typographical error in a hfs energy formula which appeared in several of our papers (Lawler et al. 2001b, 2001d, 2004). The typographical error did not affect any of our tables of hfs constants or tables of complete line component patterns (CLCPs). We are using the Casimir formula as presented in the elementary text by Woodgate (1980). This correct formula is

$$\Delta E = \frac{AK}{2} + B\frac{3K(K+1) - 4I(I+1)J(J+1)}{8I(2I-1)J(2J-1)},$$

where ΔE is the shift in wave numbers of an hfs sublevel (F, J) from the center of gravity of the fine structure level (J),

$$K = F(F+1) - J(J+1) - I(I+1),$$

F is the total atomic angular momentum, J is the total electronic angular momentum, and I is the nuclear spin. The more advanced text by Cowan (1981) has an excellent discussion of hfs, but uses a slightly different definition of the hyperfine B. Relative intensities of hyperfine components are expressed in terms of Wigner 6-j symbols by Cowan (1981). Some readers may find it more convenient to use the simple Russell-Saunders line strength formulae given in the classic text by Condon & Shortley (1935). The use of the Russell–Saunders formulae only requires substitution of F for J, J for L, and I for S.

Each RE element has its own nuclear configuration, and each first ion of these elements has a unique electronic energy structure. However, some general properties that connect many of the $Z = 57$–71 ions are worth noting. Among the seven stable odd-Z elements of this group, five of them have only one naturally-occurring isotope. Lu ($Z = 71$) has stable isotopes ^{175}Lu and ^{176}Lu, but ^{175}Lu comprises 97.4% of the solar system Lu abundance. This essentially leaves only Eu as the odd-Z RE element with multiple abundant isotopes: ^{151}Eu (47.8% of the Eu elemental abundance in the solar system), and ^{153}Eu (52.2%). Additionally, the Eu isotopic fraction appears to be relatively insensitive to the n-capture synthesis method, being nearly 50/50 in both the r-process and s-process (e.g., Sneden et al. 2002; Aoki et al. 2003). Therefore once the hyperfine patterns for odd-Z rare-earth ionized transitions are known, the spectra can be synthesized with confidence.

In contrast, all but one of the even-Z elements in this element domain have at least five naturally-occurring non-negligible isotopes (> 1% fraction in the solar system). The single exception is Ce, with just ^{140}Ce (88.5%) and ^{142}Ce (11.1%). The odd-A isotopes of these elements have non-zero nuclear magnetic moments, and thus their ionized-species transitions have usually small hfs. However, the isotopic wavelength shifts are usually undetectably small. Magain (1995) and Lambert & Allende Prieto (2002) studied the isotopic mix of Ba, a near RE element, from the Ba II 4554 Å line in one very metal-poor star, but their results had large error bars because the isotopic wavelength shifts are only ∼0.05 Å. Roederer et al. (2008) derived Sm isotopic abundance fractions from several lines of Sm II in metal-poor stars, but the isotopic splits were always <∼0.08 Å. In both of these examples the isotopic wavelength spreads are comparable to the stellar thermal and microturbulent broadening of the lines. No other RE even-Z element appears to exhibit significant isotopic broadening in spectroscopically accessible transitions (see attempts to analyze Nd II by Roederer et al.), so for most purposes their lines can be treated as single features.

Table 4 is a summary of laboratory data measured or compiled as part of this program on RE ions with locations of MR tables of log(gf) values and of CLCPs. The general discussion above is supplemented with more detailed discussions of the spectra of each RE ion below. As the quality of stellar spectra from large and very large (> 6 m) telescopes continues to improve, there will be increased opportunities for elemental abundance studies and isotopic fraction measurements on many more stars. Complete and very accurate tables of solar system isotopic fractions and nuclear moments are available, but are not included here (Böhlke et al. 2005; Stone 2005).

Lanthanum is an on odd-Z element with essentially one stable isotope, ^{139}La, with hfs from a nuclear spin $I = 7/2$ which is significant in stellar abundance work. The very low isotopic fraction of ^{138}La of 0.09% in solar system material is negligible. When our work on La II was published (Lawler et al. 2001a) we were not aware of the ApJ option to include MR tables. Table 5 is an MR version of the La II transition probability table from the 2001 paper. A set of hfs constants for ^{139}La was measured and/or compiled by Lawler et al. (2001a) and updated by Ivans et al. (2006) with an MR table of CLCPs.

Cerium is covered in this paper. It is an even-Z element with only nuclear spin $I = 0$ isotopes. Two isotopes have solar system fractions above 10%, but the isotopes shifts are generally small. There are also two rare $I = 0$ isotopes with solar system fractions < 1%. Lines of Ce II are sufficiently narrow in our FTS data that they may be treated as single component lines in stellar abundance work.

Praseodymium is discussed in the companion paper (Sneden et al. 2009). It is an odd-Z element with a single stable isotope, ^{141}Pr, with hfs from a nuclear spin $I = 5/2$ which is significant in stellar abundance work. The companion paper has a recommended set of log(gf) values and an MR table of CLCPs.

Neodymium is an even-Z element with five $I = 0$ isotopes and two $I = 7/2$ isotopes, all with fractions of 5% or more

Table 4
Master Table of Laboratory Data Measured or Compiled as Part of This Program on RE ions

Spectrum	Z	log(gf)	Isotope Data Shifts and/or hfs Constants	Location of MR Tables
La II	57	Lawler et al. 2001a	Lawler et al. 2001a; Ivans et al. 2006	log(gf): MR Table 5 below CLCP: MR Table 4 in Ivans et al. 2006
Ce II	58	This paper	...	log(gf): MR Table 2 above ...
Pr II	59	Companion paper: Sneden et al. 2009	Companion paper: Sneden et al. 2009	log(gf): Companion paper CLCP: MR Table 11 in Sneden et al. 2009
Nd II	60	Den Hartog et al. 2003	Roederer et al. 2008	log(gf): MR Table 3 in Den Hartog et al. 2003 CLCP: MR Table 5 in Roederer et al. 2008
Pm II	61	no stable isotopes	no stable isotopes	no stable isotopes
Sm II	62	Lawler et al. 2006	Roederer et al. 2008	log(gf): MR Table 2 of Lawler et al. 2006 CLCP: MR Table 4 of Roederer et al. 2008
Eu II	63	Lawler et al. 2001b	Lawler et al. 2001b; Ivans et al. 2006	log(gf): MR Table 6 below CLCP: MR Table 6 of Ivans et al. 2006
Gd II	64	Den Hartog et al. 2006	...	log(gf): MR Table 3 of Den Hartog et al. 2006 ...
Tb II	65	Lawler et al. 2001c	Lawler et al. 2001d	log(gf): MR Table 1 of Lawler et al. 2001c CLCP: MR Table 7 below
Dy II	66	Wickliffe et al. 2000	...	log(gf): MR Table 8 below ...
Ho II	67	Lawler et al. 2004	Lawler et al. 2004	log(gf): MR Table 9 below CLCP: MR Table 10 below
Er II	68	Lawler et al. 2008b	...	log(gf): MR Table 3 of Lawler et al. 2008b ...
Tm II	69	Wickliffe & Lawler 1997	...	log(gf): MR Table 11 below ...
Yb II	70	Companion paper: Sneden et al. 2009	Companion paper: Sneden et al. 2009	log(gf): Companion paper CLCP: MR Table 12 in Sneden et al. 2009
Lu II	71	Den Hartog et al. 1998; Quinet et al. 1999; Fedchak et al. 2000	Sneden et al. 2003b	log(gf): MR Table 13 below CLCP: MR Table 14 below

Note. Machine-readable (MR) tables of log(gf) values and complete line component patterns (CLCPs) are now available for these data either in the original publication or in this Appendix.

Table 5
Experimental Atomic Transition Probabilities for La II Arranged by Wavenumber from Lawler et al. (2001a)

Wavenumber (cm^{-1})	λ_{air} (Å)	Upper Level		Lower Level		Transition Probability (10^6 s^{-1})	$\log_{10}(gf)$
		Energy (cm^{-1})	J	Energy (cm^{-1})	J		
27549.30	3628.82	28565.40	4	1016.10	3	4.0 ± 0.6	−1.15
27423.91	3645.41	27423.91	1	0.00	2	43 ± 4	−0.59
27299.15	3662.07	28315.25	3	1016.10	3	3.0 ± 0.6	−1.37
26920.79	3713.54	28315.25	3	1394.46	2	10.9 ± 1.7	−0.80
26594.70	3759.08	28565.40	4	1970.70	4	49 ± 4	−0.03

(This table is available in its entirety in a machine-readable form in the online journal. A portion is shown here for guidance regarding its form and content.)

in solar system material. Some lines of Nd II have structure in our FTS data as noted in Table 3 of Den Hartog et al. (2006) but these lines tended to be weak in stellar spectra. Most lines of Nd II are sufficiently narrow in our FTS data to be treated as single component lines in stellar abundance work. Roederer et al. (2008) compiled Nd II isotope shifts and hfs constants, and published an MR tables of CLCPs. Isotopic fraction measurements on Nd in stellar abundance work have been attempted, but with only limited success because the isotope shifts are so small. Since there is no resolved structure in Nd II lines in stellar spectra, tiny center-of-gravity shifts of Nd II lines must be measured in stellar spectra to determine isotopic fractions.

Prometheum has no stable isotopes. Although there have been tentative observations of Pm II lines in stellar spectra (e.g., Cowley et al. 2004), none have been confirmed.

Samarium is an even-Z element with five $I = 0$ isotopes and two $I = 7/2$ isotopes, all with fractions of 3% or more in solar system material. Most lines of Sm II are sufficiently narrow in our FTS data to be treated as single component lines in stellar abundance work. Roederer et al. (2008) compiled Sm II isotope shifts and hfs constants, and published an MR table of CLCPs. Isotopic fraction measurements on Sm in stellar abundance work are somewhat easier than on Nd, and such measurements have been performed (Roederer et al. 2008). Small center-of-gravity shifts of Sm II lines were measured in stellar spectra to determine isotopic fractions.

Europium is an odd-Z element with two $I = 5/2$ isotopes, both with large, 47.8% and 52.2%, isotopic fractions in solar system material. When our work on Eu II was published (Lawler et al. 2001b) we did not include MR tables. Table 6 is an MR version of the Eu II transition probability table from the 2001 paper. A set of hfs constants for ^{151}Eu and ^{153}Eu was compiled by Lawler et al. (2001b). The energy levels and center-of gravity wavelengths of Eu II transition were improved by Ivans et al.

Table 6
Experimental Atomic Transition Probabilities for Eu II Arranged by Wavenumber from Lawler et al. (2001b)

Wavenumber (cm^{-1})	λ_{air} (Å)	Upper Level		Lower Level		Transition Probability (10^6 s^{-1})	$\log_{10}(gf)$
		Energy (cm^{-1})	J	Energy (cm^{-1})	J		
27104.07	3688.43	27104.07	3	0.00	4	15.0 ± 1.1	−0.67
26838.50	3724.93	26838.50	4	0.00	4	43.3 ± 2.6	−0.09
26172.83	3819.67	26172.83	5	0.00	4	135 ± 7	0.51
25587.14	3907.11	27256.35	2	1669.21	3	129 ± 6	0.17
25434.86	3930.50	27104.07	3	1669.21	3	114 ± 6	0.27

(This table is available in its entirety in a machine-readable form in the online journal. A portion is shown here for guidance regarding its form and content.)

Table 7
Hyperfine Structure Line Component Patterns for ^{159}Tb II Computed from the hfs Constants of Lawler et al. (2001b), Energy Levels of Martin et al. (1978), and the Standard Index of Air (Edlén 1953)

Wavenumber (cm^{-1})	λ_{air} (Å)	F_{upp}	F_{low}	Component Position (cm^{-1})	Component Position (Å)	Strength
32563.20	3070.059	8.5	8.5	−0.14668	0.013830	0.29338
32563.20	3070.059	8.5	7.5	0.24576	−0.023171	0.00662
32563.20	3070.059	7.5	8.5	−0.42038	0.039636	0.00662
32563.20	3070.059	7.5	7.5	−0.02794	0.002634	0.25128
32563.20	3070.059	7.5	6.5	0.31834	−0.030014	0.00877

Notes.
Center-of-gravity wavenumbers and air wavelengths, λ_{air}, are given with component positions relative to those values. Strengths are normalized to sum to 1.

(This table is available in its entirety in a machine-readable form in the online journal. A portion is shown here for guidance regarding its form and content.)

Table 8
Experimental Atomic Transition Probabilities for Dy I (Levels Have Integral J) and Dy II (Levels Have Half Integral J) from Wickliffe et al. (2000)

Wavenumber	λ_{air} (Å)	Upper Level			Lower Level			Univ. of Wisconsin			NIST		
(cm^{-1})		Energy (cm^{-1})	Parity	J	Energy (cm^{-1})	Parity	J	Transition Probability (10^6 s^{-1})	Uncert.(%)	$\log_{10}(gf)$	Transition Probability	Uncert.(%)	$\log_{10}(gf)$
34921.87	2862.69	34921.87	od	7.0	0.00	ev	8.0	7.9	6	−0.84	...	...	...
33311.52	3001.09	33311.52	od	7.0	0.00	ev	8.0	1.45	6	−1.53	...	...	...
33165.77	3014.28	33165.77	od	8.0	0.00	ev	8.0	1.18	7	−1.56	...	...	...
33035.57	3026.16	33035.57	od	9.5	0.00	ev	8.5	3.82	6	−0.98	...	...	...
32490.90	3076.89	33319.21	od	6.5	828.31	ev	7.5	1.35	10	−1.57	...	...	...

(This table is available in its entirety in a machine-readable form in the online journal. A portion is shown here for guidance regarding its form and content.)

Table 9
Experimental Atomic Transition Probabilities for Ho II Arranged by Wavenumber from Lawler et al. (2004)

Wavenumber (cm^{-1})	λ_{air} (Å)	Upper Level		Lower Level		Transition Probability (10^6 s^{-1})	$\log_{10}(gf)$	
		Energy (cm^{-1})	J	Energy (cm^{-1})	J		This Expt.	Other
30918.86	3233.34	31556.61	7	637.75	7	4.1 ± 0.8	−1.02	
29899.58	3343.57	29899.58	7	0.00	8	14.1 ± 1.1	−0.45	−0.54[a]
29450.17	3394.59	35067.62	6	5617.46	7	16.1 ± 1.1	−0.44	
29412.51	3398.94	29412.51	8	0.00	8	87 ± 5	0.41	0.27[b]
29325.35	3409.04	29325.35	7	0.00	8	3.05 ± 0.21	−1.10	

Notes.
[a] VALD database as described in Kupka et al. (1999), value determined using the method of Magazzù & Cowley (1986).
[b] VALD database as described in Kupka et al. (1999), value originally from Gorshkov & Komarovskii (1979).

(This table is available in its entirety in a machine-readable form in the online journal. A portion is shown here for guidance regarding its form and content.)

(2006) and CLCPs were provided in MR Table 6 of that paper. Astrophysical data on halo stars from modern large telescopes have now reached the level of quality that isotopic abundances of Eu can be determined with some accuracy and precision (e.g., Sneden et al. 2002; Aoki et al. 2003). Evidence to date supports a uniform isotopic mix from all *r*-process events. The lines of Eu II connected to ground and lowest metastable levels are ideal for such studies. The unpaired s-electron of these two levels yields both large isotope shifts from the finite nuclear size (field shifts) and wide hfs. Isotope shifts and hfs yield resolvable structure in Eu II lines in stellar spectra, which is much easier to measure than the small wavelength shifts of Sm II or Nd II lines due to varying isotopic fractions.

Gadolinium is an even-Z element with five $I = 0$ isotopes and two $I = 3/2$ isotopes. The two lightest $I = 0$ isotopes have rather low fractions $< 2.5\%$ in solar system material. Most lines of Gd II are sufficiently narrow in our FTS data to be treated as single component lines in stellar abundance work. The widths of line profiles in our highest resolution FTS data vary, and in a few cases the profiles have partially resolved structure. Although it is

Table 10
Hyperfine Structure Line Component Patterns for Ho II Computed Using hfs Constants and Improved Energy Levels from Lawler et al. (2004) and the Standard Index of Air (Edlén 1953)

Wavenumber (cm^{-1})	λ_{air} (Å)	F_{upp}	F_{low}	Component Position (cm^{-1})	Component Position (Å)	Strength
30918.859	3233.3387	10.5	10.5	0.81266	−0.084984	0.17569
30918.859	3233.3387	10.5	9.5	0.80394	−0.084073	0.00764
30918.859	3233.3387	9.5	10.5	0.46722	−0.048860	0.00764
30918.859	3233.3387	9.5	9.5	0.45850	−0.047949	0.14620
30918.859	3233.3387	9.5	8.5	0.45885	−0.047985	0.01283

Note. Center-of-gravity wavenumbers and air wavelengths, λ_{air}, are given with component positions relative to those values. Strengths are normalized to sum to 1.

(This table is available in its entirety in a machine-readable form in the online journal. A portion is shown here for guidance regarding its form and content.)

Table 11
Experimental Atomic Transition Probabilities for Tm II from Wickliffe & Lawler (1997)

Wavenumber (cm^{-1})	λ_{air} (Å)	Upper Level			Lower Level			Transition	Uncert.(%)	$\log_{10}(gf)$
		Energy (cm^{-1})	Parity	J	Energy (cm^{-1})	Parity	J	Probability (10^6 s^{-1})		
34913.84	2863.35	34913.84	ev	3	0.00	od	4	1.05	8	−2.04
34842.39	2869.22	47299.68	od	7	12457.29	ev	6	225	6	0.62
34634.42	2886.45	34871.37	ev	4	236.95	od	3	1.16	11	−1.88
34580.75	2890.93	34580.75	ev	5	0.00	od	4	5.23	5	−1.14
34307.52	2913.96	34307.52	ev	4	0.00	od	4	1.11	5	−1.89

(This table is available in its entirety in a machine-readable form in the online journal. A portion is shown here for guidance regarding its form and content.)

not possible today, it may at some point in the future be possible to observe the isotopic mixture of Gd in a metal-poor halo star.

Terbium is an on odd-Z element with one stable isotope, ^{159}Tb, with hfs from a nuclear spin $I = 3/2$ which is significant in stellar abundance work. Lawler et al. (2001d) published a large set of hfs constants. CLCPs for lines of Tb II are in MR Table 7.

Dysprosium is an even-Z element with five $I = 0$ isotopes and two $I = 5/2$ isotopes. The three lightest $I = 0$ isotopes have rather low fractions $< 2.5\%$ in solar system material. Although some lines have detectable structure, most lines of Dy II are sufficiently narrow in our FTS data to be treated as single component lines in stellar abundance work. Wickliffe et al. (2000) measured a large set of Dy I and Dy II transition probabilities in this effort on RE species. This work on Dy was done jointly with NIST and comparisons of independent branching fraction measurements were performed. Both the Univ. of Wisconsin (UW) and NIST transition probabilities are based on the same radiative lifetimes measured at UW using time-resolved LIF. Wickliffe et al. published a merged table of Dy I and Dy II transition probabilities with both UW and NIST measurements. This table has been reconstructed here as an MR Table 8.

Holmium is an odd-Z element with a single stable isotope, ^{165}Ho, and hfs from a nuclear spin $I = 7/2$ which is significant in stellar abundance work. The high line density of Ho I and Ho II in combination with wide hfs has inhibited analysis of Ho II. Lawler et al. (2004) focused their efforts on the low-lying levels which are connected by strong "resonance-like" transitions. They reported new transition probability measurements based on radiative lifetimes from LIF in combination with branching fractions from FTS data, a small set of improved energy levels from FTS data for better center-of-gravity wavelengths, and hfs constants from FTS data for the levels of interest. Their table of transition probabilities is reproduced as an MR Table 9 below, and MR Table 10 includes CLCPs for the strong "resonance-like" lines of Ho II.

Erbium is an even-Z element with five $I = 0$ isotopes and one I= 7/2 isotope. The two lightest $I = 0$ isotopes have rather

Table 12
Improved Lu II Energy Levels (± 0.008 cm^{-1}) and NIST (Martin et al. 1978) Energy Levels for Comparison

Energy (cm^{-1}) This Expt.	NIST	J
0.000	0.00	0
11796.108	11796.24	1
12435.229	12435.32	2
14198.978	14199.08	3
17332.428	17332.58	2
27264.269	27264.40	0
28503.149	28503.16	1
32453.115	32453.26	2
41224.821	41224.96	2
44918.529	44918.68	3
48536.758	48536.83	4
45458.326	45458.56	2

low fractions $< 2\%$ in solar system material. Although some lines have detectable structure, most lines of Er II are sufficiently narrow in our FTS data to be treated as single component lines in stellar abundance work. Some of the IR lines studied by Lawler et al. (2008b) have detectable isotopic structures, but these lines are so weak with such high excitation potentials that there is no hope of astrophysical detections in the foreseeable future.

Thulium is an odd-Z element with one stable isotope, ^{169}Tm. This isotope has a nuclear spin of $I = 1/2$. Although some lines have detectable structure, most lines of Tm II are sufficiently narrow in our FTS data to be treated as single component lines in stellar abundance work. Wickliffe and Lawler (1997) measured a large set of Tm I and Tm II transition probabilities in this effort on RE species. Their data on Tm II are included below as an MR Table 11.

Ytterbium is discussed in the companion paper (Sneden et al. 2009). It is an even-Z element with five $I = 0$ isotopes, one $I = 1/2$ isotope, and one $I = 5/2$ isotope. The lightest two $I = 0$ isotopes have rather low fractions, $< 3.1\%$, in solar system material. Only two Yb II resonance lines from the same multiplet are useful in abundance studies and thus an MR table of

Table 13
Experimental Atomic Transition Probabilities for Lu II from Odd-Parity Upper Levels Organized by Increasing Wavelength in Air

λ_{air} (Å)	Upper Level		Lower Level		Transition Probability (10^6 s^{-1})	$\log_{10}(gf)$
	Energy (cm^{-1})	J	Energy (cm^{-1})	J		
2571.23	53079.33	3	14199.08	3	39.8 ± 2.7	−0.56
2754.17	48733.19	3	12435.32	2	103 ± 7	−0.09
2796.63	53079.33	3	17332.58	2	181 ± 9	0.17
2894.84	48733.19	3	14199.08	3	186 ± 12	0.21
2911.3915	48536.758	4	14198.978	3	245 ± 16	0.45
3077.6109	44918.529	3	12435.229	2	131 ± 7	0.12
3254.3173	44918.529	3	14198.978	3	64 ± 4	−0.15
3397.0669	41224.821	2	11796.108	1	75 ± 5	−0.19
3472.4832	41224.821	2	12435.229	2	71 ± 5	−0.19
3507.3810	28503.149	1	0.000	0	12.5 ± 1.1	−1.16
3623.9806	44918.529	3	17332.428	2	11.9 ± 1.4	−0.79
4184.2533	41224.821	2	17332.428	2	21.0 ± 2.0	−0.56
4839.6201	32453.115	2	11796.108	1	0.45 ± 0.05	−2.10
4994.1393	32453.115	2	12435.229	2	4.73 ± 0.28	−1.05
5476.6884	32453.115	2	14198.978	3	21.2 ± 1.1	−0.32
5983.8429	28503.149	1	11796.108	1	4.3 ± 0.4	−1.16
6221.8596	28503.149	1	12435.229	2	9.9 ± 0.9	−0.76
6463.1065	27264.269	0	11796.108	1	15.4 ± 0.8	−1.01
8459.16	41224.96	2	29406.70	2	2.5 ± 0.5	−0.87

Notes.
Updated energy levels from Table 12 are used for transitions if available both for the upper and lower levels, otherwise NIST (Martin et al. 1978) energy levels are used. Wavelengths are computed using the standard index of air (Edlén 1953).

(This table is also available in a machine-readable form in the online journal.)

Table 14
Hyperfine Structure Line Component Patterns for ^{175}Lu II Computed from the hfs constants of Sneden et al. (2003b), Energy Levels of Table 12, and the Standard Index of Air (Edlén 1953)

Wavenumber (cm^{-1})	λ_{air} (Å)	F_{upp}	F_{low}	Component Position (cm^{-1})	Component Position (Å)	Strength
34337.780	2911.3915	7.5	6.5	−0.53033	0.044968	0.22222
34337.780	2911.3915	6.5	6.5	−0.62922	0.053353	0.02618
34337.780	2911.3915	6.5	5.5	−0.22156	0.018786	0.16827
34337.780	2911.3915	5.5	6.5	−0.67036	0.056841	0.00160
34337.780	2911.3915	5.5	5.5	−0.26270	0.022274	0.04196

Notes.
Center-of-gravity wavenumbers and air wavelengths, λ_{air}, are given with component positions relative to those values. Strengths are normalized to sum to 1. Table 14 is available in its entirety via the link to the machine-readable version above.

(This table is available in its entirety in a machine-readable form in the online journal. A portion is shown here for guidance regarding its form and content.)

transition probabilities is unnecessary. The unpaired s-electron of the ground level yields large isotope shifts and hfs. Isotopic and hfs are not negligible in stellar abundance work on Yb II. The companion paper has recommended log(*gf*) values and an MR table of CLCPs.

Lutetium is an odd-*Z* element with one dominant stable isotope, ^{175}Lu, with hfs from a nuclear spin $I = 7/2$ which is significant in stellar abundance work. The low isotopic fraction of ^{176}Lu of 2.59% in solar system material is negligible given the generally low abundance of Lu and quality of stellar spectra available today. During a search for Lu in metal-poor stars, it became apparent that the NIST energy levels (Martin et al. 1978) are not as accurate as the NIST energy levels for many other species. Energy levels from older measurements using photographic techniques on species with wide hfs often have this problem. Table 12 presents new energy level measurements for some of the low-lying levels of Lu II of both parities. Lutetium was studied early in this project on RE ions, shortly after Bord et al. (1998) found a clean Lu II line in the solar spectrum at 6221 Å. Den Hartog et al. (1998) measured the upper level lifetime of this line using LIF and the branching fractions of lines from this level using FTS data to determine accurate transition probabilities. Shortly thereafter, additional branching fractions from FTS data were reported by Quinet et al. (1999) and additional radiative lifetimes from time-resolved LIF were reported by Fedchak et al. (2000). In this early phase of the RE project we collaborated more closely with atomic theorists and performed numerous comparisons of experimental and theoretical transition probabilities. With only two valence electrons, Lu II is a particularly simple RE spectrum with minimal configuration mixing. However, both core polarization and relativistic effects are important in Lu II like other RE spectra. At this time we are of the opinion that careful branching fraction measurements from FTS data in combination with radiative lifetimes from LIF generally yield better RE transition probabilities than can be computed using ab initio quantum methods. We therefore recommend the Lu II transition probabilities of Table 13 that were determined by combining branching fractions from FTS data with radiative lifetimes from our time-resolved LIF experiment. Sneden et al. (2003b) measured a set of hfs constants from FTS data for

levels of ^{175}Lu. For the user's convenience MR Table 14 includes CLCPs for lines of ^{175}Lu II. The reader should note that the components from the rare (2.59%) isotope ^{176}Lu are not included in Table 14. New energy levels from Table 12 are included in Tables 13 and 14 if available for both the upper and lower levels of the transition, otherwise energy levels from Martin et al. (1978) are used. Air wavelengths are computed from those energy levels using the standard index of air (Edlén 1953).

REFERENCES

Adams, D. L., & Whaling, W. 1981, J. Opt. Soc. Am., 71, 1036
Aoki, W., Honda, S., Beers, T. C., & Sneden, C. 2003, ApJ, 586, 506
Arlandini, C., Käppeler, F., Wisshak, K., Gallino, R., Lugaro, M., Busso, M., & Straniero, O. 1999, ApJ, 525, 886
Biémont, E., & Quinet, P. 2005, J. Electron Spectrosc. Relat. Phenom., 144, 23
Böhlke, J. K., de Laeter, J. R., De Bièvre, P., Hidaka, H., Peiser, H. S., Rosman, K. J. R., & Taylor, P. D. P. 2005, J. Phys. Chem. Ref. Data, 34, 57
Bord, D. J., Cowley, C. R., & Mirijanian, D. 1998, Sol. Phys., 178, 221
Brault, J. W. 1976, J. Opt. Soc. Am., 66, 1081
Burris, D. L., Pilachowski, C. A., Armandroff, T. E., Sneden, C., Cowan, J. J., & Roe, H. 2000, ApJ, 544, 302
Condon, E. U., & Shortley, G. H. 1935, The Theory of Atomic Spectra (Cambridge: Cambridge Univ. Press), 238
Cowley, C. R., Bidelman, W. P., Hubrig, S., Mathys, G., & Bord, D. J. 2004, A&A, 419, 1087
Cowan, J. J., Sneden, C., Truran, J. W., & Burris, D. L. 1996, ApJ, 460, L115
Cowan, J. J., et al. 2002, ApJ, 572, 861
Cowan, R. D. 1981, The Theory of Atomic Structure and Spectra (Berkeley, CA: Univ. of California Press), 508
Danzmann, K., & Kock, M. 1982, J. Opt. Soc. Am., 72, 1556
Delbouille, L., Roland, G., & Neven, L. 1973, Photometric Atlas of the Solar Spectrum from lambda 3000 to lambda 10000 (Liège, Inst. d'Ap.: Univ. de Liège)
Den Hartog, E. A., Curry, J. J., Wickliffe, M. E., & Lawler, J. E. 1998, Sol. Phys., 178, 239
Den Hartog, E. A., & Lawler, J. E. 2008, J. Phys. B: At. Mol. Opt. Phys., 41, 045701
Den Hartog, E. A., Lawler, J. E., Sneden, C., & Cowan, J. J. 2003, ApJS, 148, 543
Den Hartog, E. A., Lawler, J. E., Sneden, C., & Cowan, J. J. 2006, ApJS, 167, 292
Edlén, B. 1953, J. Opt. Soc. Am., 43, 339
Fawcett, B. C. 1990, At. Nucl. Data Tables, 46, 217
Fedchak, J. A., Den Hartog, E. A., Lawler, J. E., Palmeri, P., Quinet, P., & Biémont, E. 2000, ApJ, 542, 1109
Grevesse, N., Asplund, M., & Sauval, A. J. 2007, Space Sci. Rev., 130, 105
Grevesse, N., & Sauval, A. J. 1999, A&A, 347, 348
Grevesse, N., & Sauval, A. J. 2002, Adv. Space. Res., 30, 3
Grigoriev, I. S., & Melikhov, E. Z. 1997, Handbook of Physical Quantities (Boca Raton, FL: CRC Press), 516
Hannaford, P., Lowe, R. M., Grevesse, N., Biémont, E., & Whaling, W. 1982, ApJ, 261, 736
Hashiguchi, S., & Hasikuni, M. 1985, J. Phys. Soc. Japan, 54, 1290
Hill, V., et al. 2002, A&A, 387, 560
Holweger, H., & Müller, E. A. 1974, Sol. Phys., 39, 19
Irwin, A. W. 1981, ApJS, 45, 621
Ivans, I. I., Simmerer, J., Sneden, C., Lawler, J. E., Cowan, J. J., Gallino, R., & Bisterzo, S. 2006, ApJ, 645, 613
Kurucz, R. L. 1998, in IAU Symp. 189, Fundamental Stellar Properties: The Interaction between Observation and Theory, ed. T. R. Bedding, A. J. Booth, & J. Davis (Dordrecht: Kluwer), 217
Lambert, D. L., & Allende Prieto, C. 2002, MNRAS, 335, 325
Langhans, G., Schade, W., & Helbig, V. 1995, Z. Phys. D, 34, 155
Lawler, J. E., Bonvallet, G., & Sneden, C. 2001a, ApJ, 556, 452
Lawler, J. E., Den Hartog, E. A., Labby, Z. E., Sneden, C., Cowan, J. J., & Ivans, I. I. 2007, ApJS, 169, 120
Lawler, J. E., Den Hartog, E. A., Sneden, C., & Cowan, J. J. 2006, ApJS, 162, 227
Lawler, J. E., Den Hartog, E. A., Sneden, C., & Cowan, J. J. 2008a, Can. J. Phys., 86, 1033
Lawler, J. E., Sneden, C., & Cowan, J. J. 2004, ApJ, 604, 850
Lawler, J. E., Sneden, C., Cowan, J. J., Wyart, J.-F., Ivans, I. I., Sobeck, J. S., Stockett, M. H., & Den Hartog, E. A. 2008b, ApJS, 178, 71
Lawler, J. E., Wickliffe, M. E., Cowley, C. R., & Sneden, C. 2001c, ApJS, 137, 341
Lawler, J. E., Wickliffe, M. E., Den Hartog, E. A., & Sneden, C. 2001b, ApJ, 563, 1075
Lawler, J. E., Wyart, J.-F., & Blaise, J. 2001d, ApJS, 137, 351
Li, Z. S., Lundberg, H., Wahlgren, G. M., & Sikström, C. M. 2000, Phys. Rev. A, 62, 032505
Lodders, K. 2003, ApJ, 591, 1220
Malcheva, G., Blagoev, K., Mayo, R., Ortiz, M., Xu, H. L., Svanberg, S., Quinet, P., & Biémont, E. 2006, MNRAS, 367, 754
Magain, P. 1995, A&A, 297, 686
Martin, W. C., Sugar, J., & Musgrove, A. 2000, NIST Atomic Spectra Database, (http://physics.nist.gov/PhysRefData/ASD/index.html)
Martin, W. C., Zalubas, R., & Hagan, L. 1978, Atomic Energy Levels The Rare Earth Elements, NSRDS NBS 60 (Washington, DC: US Govt Printing Office), 70
Moore, C. E., Minnaert, M. G. J., & Houtgast, J. 1966, The Solar Spectrum 2934 Å to 8770 Å, NBS Monograph 61 (Washington, DC: US Govt Printing Office)
Palmeri, P., Quinet, P., Wyart, J.-F., & Biémont, E. 2000, Phys. Scr., 61, 323
Quinet, P., Palmeri, P., Biémont, E., McCurdy, M. M., Rieger, G., Pinnington, E. H., Wickliffe, M. E., & Lawler, J. E. 1999, MNRAS, 307, 934
Rehse, S. J., Li, R., Scholl, T. J., Sharikova, A., Chatelain, R., Holt, R. A., & Rosner, S. D. 2006, Can. J. Phys., 84, 723
Roederer, I. U., Lawler, J. E., Sneden, C., Cowan, J. J., Sobeck, J. S., & Pilachowski, C. A. 2008, ApJ, 675, 723
Simmerer, J., Sneden, C., Cowan, J. J., Collier, J., Woolf, V. M., & Lawler, J. E. 2004, ApJ, 617, 1091
Smith, V. V., Cunha, K., & Lambert, D. L. 1995, AJ, 110, 2827
Sneden, C. 1973, ApJ, 184, 839
Sneden, C., Basri, G., Boesgarrd, A. M., Brown, J. A., Carney, B. W., Kraft, R. P., Smith, V., & Suntzeff, N. B. 1995, PASP, 107, 997
Sneden, C., Cowan, J. J., & Lawler, J. E. 2003a, Nucl. Phys. A, 718, 29c
Sneden, C., Cowan, J. J., Lawler, J. E., Burles, S., Beers, T. C., & Fuller, G. M. 2002, ApJ, 566, L25
Sneden, C., Lawler, J. E., Cowan, J. J., Ivans, I. I., & Den Hartog, E. A. 2009, ApJS, 182, 80
Sneden, C., McWilliam, A., Preston, G. W., Cowan, J. J., Burris, D. L., & Armosky, B. J. 1996, ApJ, 467, 819
Sneden, C., et al. 2003b, ApJ, 591, 936
Stone, N. J. 2005, At. Data Nucl. Data Tables, 90, 75
Westin, J., Sneden, C., Gustafsson, B., & Cowan, J. J. 2000, ApJ, 530, 783
Whaling, W., Carle, M. T., & Pitt, M. L. 1993, J. Quant. Spectrosc. Radiat. Transfer, 50, 7
Wickliffe, M. E., & Lawler, J. E. 1997, J. Opt. Soc. Am. B, 14, 737
Wickliffe, M. E., Lawler, J. E., & Nave, G. 2000, J. Quant. Spectrosc. Radiat. Transfer, 66, 363
Woolf, V. M., Tomkin, J., & Lambert, D. L. 1995, ApJ, 453, 660
Woodgate, G. K. 1980, Elementary Atomic Structure,2nd edn. (Oxford: Clarendon), 184
Xu, H. L., Persson, A., & Svanberg, S. 2003, Eur. Phys. J. D, 23, 233
Zhang, Z. G., Svanberg, S., Jiang, Z., Palmeri, P., Quinet, P., & Biémont, E. 2001, Phys. Scr., 63, 122